Distinguishing magmatic and metamorphic processes in peralkaline rocks of the Norra Kärr complex (Southern Sweden) using textural and compositional variations of clinopyroxene and eudialyte-group minerals.

Atanasova, P.; Marks, M. A. W.; Kraise, J.; Gutzmer, J.; Markl, G.; Heinig, T.;

Originally published:

May 2017

Journal of Petrology 58(2017), 361-384

DOI: https://doi.org/10.1093/petrology/egx019

Distinguishing magmatic and metamorphic processes in peralkaline rocks of the Norra Kärr complex (Southern Sweden) using textural and compositional variations of clinopyroxene and eudialyte-group minerals.

Corresponding author: Atanasova P.

Helmholtz-Zentrum Dresden - Rossendorf, Helmholtz Institute Freiberg for Resource Technology, 09599 Freiberg, Saxony, Germany

Tel.: +49 (0) 351 260-4406, Fax: +49 (0) 351 260-14402, e-mail: p.atanasova@hzdr.de

Universität Tübingen, Fachbereich Geowissenschaften, 72074 Tübingen, Germany

Marks M. A. W., Markl G.

Universität Tübingen, Fachbereich Geowissenschaften, 72074 Tübingen, Germany

Heinig T., Krause J., Gutzmer J.

Helmholtz-Zentrum Dresden - Rossendorf, Helmholtz Institute Freiberg for Resource Technology, 09599 Freiberg, Saxony, Germany

Technical University Bergakademie Freiberg, Department of Mineralogy, 09596 Freiberg, Germany

Running Title: Magmatic and Metamorphic Processes in the Norra Kärr Alkaline Complex

Abstract

The 1.49 Ga old Norra Kärr complex in Southern Sweden contains rocks characterized by a very high ratio of (Na+K)/Al ≥ 1.2 and a complex and highly unusual mineralogy, including rock-forming catapleiite, eudialyte-group minerals as well as minor rinkite- and britholite-group minerals. In contrast to other well-studied examples of agpaitic rocks, the Norra Kärr rocks have been deformed and partially metamorphosed during the Sveconorvegian/Grenvillian orogeny, and are now preserved in a westward dipping synform. Magmatic and metamorphic processes at the Norra Kärr complex are distinguished by combining rock fabrics of clinopyroxene and eudialyte-group minerals. Both mineral groups are stable over a large P-T range, which makes them excellent monitors of the geochemical evolution of such systems and enables the reconstruction of magmatic and subsequent metamorphic conditions.

The magmatic mineral assemblage crystallized from a subsolvus syenite at continuously decreasing temperatures (700 - 450ºC) and silica activity (0.6 - 0.3). Due to initially relatively low peralkalinity and reducing conditions, Zr was first incorporated in Zr-aegirine. Subsequent destabilization of the latter indicates increasing peralkalinity, oxygen fugacity and water activity, which resulted in the crystallization of early magmatic catapleiite. Crystallization of presumably later magmatic Mn- and REE-poor eudialyte-group minerals, happened as soon as sufficient Cl, REE and HFSE were enriched in the residual melt.

Metamorphic conditions during the Sveconorvegian/Grenvillian orogeny are constrained to T between 400 - 550ºC and a_{SiO2} range of 0.25 - 0.4. Due to deformation and interaction with fluids, post-magmatic Al-rich aegirine as well as post-magmatic eudialyte-group minerals enriched in REE, Y and Mn formed. Subsequently, the eudialyte-group minerals were destabilized and decomposed to post-magmatic catapleiite and secondary REE-

bearing minerals. During the whole history of the complex, a_{SiO2} remains very similar, indicating very little interaction with the surrounding granitic rocks.

Regardless of the intense deformation due to folding of the Norra Kärr body during the Sveconorvegian/Grenvillian orogeny, indications for primary magmatic layering of the intrusion are retained on the deposit scale. In addition, the compositional changes of magmatic eudialyte-group minerals from the outer to the inner subunit indicate a primary geochemical evolution feature due to fractional crystallization.

Keywords: deformed nepheline syenite; rare earth elements; clinopyroxene, eudialyte-group minerals

INTRODUCTION

During the last decade the economic interest in high field strength elements (HFSE) and rare earth elements (REE) increased due to their broad application in high-tech products. In addition to carbonatites, alkaline and especially peralkaline rocks (molar Na+K > Al) are particularly enriched in HFSE and comprise one of the most promising sources for future REE supply (e.g., Mitchell, 2015; Smith et al., 2015; Goodenough et al., 2016). The extraordinary enrichment of HFSE and REE in such rocks was explained by the high alkalinity and the reducing conditions during crystallization of the magma, which minimizes the loss of volatile components and maximizes the ore precipitation potential during magmatic differentiation (e.g., Kogarko, 1990; Marks et al., 2011).

This study investigates peralkaline rocks of the Norra Kärr complex in southern Sweden, which are characterized by an unusual mineralogy including rock-forming catapleiite, eudialyte-group minerals (EGM) and minor REE-bearing minerals of the rinkite- and britholite-groups (Adamson, 1944; Eckermann, 1968; Sjöqvist et al., 2013). Such lithologies are classified as agpaitic rocks, a term originally introduced by Ussing (1912) and later complemented by Sørensen (1960, 1997) and Marks et al. (2011). Minerals of the eudialyte group are the most common index minerals in agpaitic rocks (e.g., Sørensen, 1997; Schilling et al., 2011b). Such minerals can incorporate significant concentrations of more than 30 elements, including Zr, Nb and naturally occurring lanthanides and Y, with LREE being commonly more abundant than the HREE.

Unlike other well-studied examples of agpaitic complexes such as the Ilímaussaq complex in Greenland (see recent reviews by Sørensen et al., 2006; Upton, 2013; Marks & Markl, 2015; Dostal, 2015) or the Lovozero and Khibina complexes in Russia (e.g. Kogarko

et al., 1982; Kogarko, 1987; Pekov, 1998; Arzamastsev et al., 2001, 2005), the igneous Norra Kärr body has been deformed and partially recrystallized during subsequent metamorphic events. This specific feature is used to amplify the restricted knowledge on the behavior of agpaitic rocks during metamorphism, which is to date mainly limited to studies of: the Red Wine and Kipawa complexes in Canada (Curtis & Gittins, 1979; Curtis & Currie, 1981; Currie & van Breemen, 1996; van Breemen & Currie, 2004); nepheline syenites in Malawi (e.g. Woolley et al., 1996); and peralkaline gneisses in India (Nanda et al., 2008; Goswami & Basu, 2013; Chakrabarty et al., 2016). We present detailed observations on rock and mineral textures combined with compositional data for the major rock-forming minerals to provide some direct insight into the petrological and geochemical processes accompanied by the deformation and metamorphism of agpaitic rocks.

GEOLOGICAL SETTING

The Norra Kärr complex is located approx. 2 km E of Lake Vättern, approx. 15 km NNE of the township of Gränna in Southern Sweden (Fig. 1). It is situated in the Trans-scandinavian Igneous Belt, which intruded into the Svecofennian domain of Fennoscandia in the course of juvenile crust reworking between 1.85–1.75 Ga (Andersson et al., 2007 and references therein). The Trans-scandinavian Igneous Belt rocks form a voluminous array of monzodioritic to granitic batholiths of alkali-calcic to calc-alkaline composition (Högdahl et al., 2004; Fig. 1). They extend over ca. 1400 km from NW Norway to SE Sweden. Significant igneous activity between 1.65–1.50 Ga was responsible for the formation of an active margin along the south-western border of the Fennoscandian Shield (McLelland, 1989). From ca. 1470 Ma onwards A- and I-type granitoids and syenitoids were emplaced in a typical

volcanic-arc setting, marking the pre-collisional stage of the Danopolonian or Hallandian orogeny in the area east and southeast of Lake Vättern (Brander, 2011, Brander & Söderlund, 2009). In the time of 1.5-1.4 Ga two possible settings for intra-cratonic magmatism are discussed in the literature, an anorogenic and an orogenic extension. Aberg (1988) interpreted the emplacement of alkali-calcic and calc-alkaline intrusions into the southernmost parts of the Trans-scandinavian Igneous Belt as a product of continental rifting between 1.48 and 1.35 Ga (Aberg et al., 1984; 1985a; 1985b; Smellie & Stuckless, 1985).

During the period of around 1140 – 900 Ma wide areas of the southern and central Trans-scandinavian Igneous Belt, as well as broad areas of south-western Fennoscandia were subject to the collision of Fennoscandia with Amazonia during the Grenvillian/Sveconorwegian orogeny (e.g. Bingen et al., 2008). These areas form today the Sveconorwegian orogenic belt. The area east of Lake Vättern belongs to the frontal zone of the orogen and was mainly affected by metamorphism during the late stages of the orogeny, the so-called Falkenberg and Dalane phases (e.g. by Bingen et al., 2008 and references therein). During the Falkenberg phase (980-970 Ma) crustal thickening and associated eclogite facies conditions affected the Fennoscandian crust to at least 50 km depth. This was followed by decompression, relaxation and gravitational collapse during the Dalane phase at 970-900 Ma (Bingen et al., 2006; 2008; Möller et al., 2007). During this time the N-S trending Protogine Zone was formed as a steep, sheer zone at the very front of the Sveconorvegian orogen (Andréasson & Rodhe, 1994; Wahlgren et al., 1994; Söderlund et al., 2004).

The Norra Kärr complex

126 The relatively small Norra Kärr complex covers an area of approx. 350 x 1100 m and is
127 located in the Växjö Granite Suite (TIB I), between the Vimmerby Batholith in the east and
128 the major Protogine shear zone (PZ) in the west (Fig. 1b). The body is preserved within a
129 westwards dipping (approx. 40°) synform (Fig. 2), deformed by moderate E-W and late, weak
130 N-S directed compression under ductile conditions (Rankin, 2011).

131 The granitic host rocks at the western contact of the Norra Kärr complex and some
132 deeper parts in the east (only known from drilling cores) exhibit clear signs of fenitization
133 (Adamson, 1944; Eckermann, 1968; Sjöqvist et al., 2015). These fenites are up to 100 m wide
134 massive horizons, but also occur as decimeter-thick veins in the surrounding granite. They are
135 characterized by the absence of quartz, which is replaced by albite, magnetite, hematite and
136 fluorite, and the replacement of biotite by aegirine (Adamson, 1944; Sjöqvist et al., 2015).
137 Fenitization of the alkaline rocks itself is less prominent and rarely occurs in the outer
138 subunit, only at the direct contact to the fenitized host rocks. Recently, the fenitization of the
139 granitic gneisses was determined to have a U-Pb zircon age of 1.49 ± 0.01 Ga (Sjöqvist et al.,
140 2014), which is interpreted coeval with the age of magmatic emplacement of the Norra Kärr
141 complex in a presumably pre-collisional rifting setting. Younger ages determined by Sjöqvist
142 et al. (2014) constrain the deformation during the Sveconorvegian orogeny from 1148 ± 5 Ma
143 onwards. At Norra Kärr neither the surrounding country rocks (granitic- to- syenitic gneisses)
144 nor the metamorphosed syenites of the complex itself provide any clear evidence indicating
145 the grade of metamorphism of the complex. Regional geological studies (Wahlgren &
146 Stephens, 2004) report lower greenschist facies conditions for the area to the East of Lake
147 Vättern and the Protogine shear Zone (Fig. 1). Considering this and the actual position of the
148 complex within this major shear zone (Fig. 1), moderate- to- high greenschist facies
149 conditions can be assumed.

150 For this study, the peralkaline rocks of the Norra Kärr complex were collectively
151 classified as meta-nepheline syenites (after Gillespie & Styles, 1999). The most common rock
152 type (85 vol.% of the exposed area), the so-called grennaite (Adamson, 1944) is a catapleiite-
153 and EGM-bearing aegirine meta-nepheline syenite (Fig. 2). The texture of this unit varies
154 systematically across the deposit (Figs 3, 4 and Electronic Appendix 1). On the basis ofthe
155 frequency of medium- to- coarse-grained lenses and bands or schlieren (Törnebohm, 1906;
156 Adamson, 1944; Sjöqvist et a1., 2015), the frequency of catapleiite and the degree of
157 deformation, the following three subunits with gradual transitions between them are
158 distinguished: The central part (inner subunit) was strongly foliated (Figs 3a-b and 4a-c) and
159 is best described as an aegirine leuco-meta-nepheline syenite (a.k.a. migmatitic grennaite;
160 lithologic nomenclature by Tasman Metals, Sjöqvist et a1., 2013). This area is surrounded by
161 a zone rich in pegmatoidal schlieren (mid subunit, Figs 3e-h and 4e and i-k) named pegmatite-
162 bearing aegirine meta-nepheline syenite (a.k.a. pegmatitic grennaite; Adamson, 1944). The
163 border area (outer subunit, Figs 3c and 4f-h) of the complex is defined by a foliated
164 catapleiite-bearing aegirine meta-nepheline syenite (a.k.a. catapleiite grennaite; Adamson,
165 1944).

166 Minor rock types of the Norra Kärr complex include the strongly folded fluoro-
167 leakeite-aegirine meta-nepheline syenite (previously called kaxtorpite, Fig. 4d), the aegirine-
168 amphibole-biotite meta-nepheline syenite (a.k.a. pulaskite) and the arfvedsonite-aegirine
169 meta-nepheline syenite (former lakarpite), well-known from the discovery outcrop of Norra
170 Kärr (Sjöqvist et a1., 2013).

171 The most common deformation features of all rock types include the alignment and
172 stretching of certain minerals (e.g. clinopyroxene, EGM, catapleiite, Fig. 4a-e) and the
173 presence of porphyroclasts (mainly microcline, Fig. 4f-h), which have tails of recrystallized

material (Fig. 4h). They are commonly preserved in a finer-grained, probably recrystallized matrix and form typical shear related patterns (sigma- and delta-clast, Fig. 4f).

PETROGRAPHY

The phase assemblages and micro-textural characteristics of the investigated samples are described in the following. A list of investigated samples is given in Table 1, sample locations are indicated in Fig.2. The modal mineralogy of the main subunits is summarized in Table 2.

Catapleiite-and EGM-bearing aegirine meta-nepheline syenite (grennaite)

Inner subunit (aegirine leuco-meta-nepheline syenite)

This unit displays strong foliation and in places intense folding, with rather common crenulated foliation and gneissic textures (Figs 3a and b and 4a-c). The main felsic minerals are subhedral- to- anhedral and fine-grained albite (up to 30 wt.%), microcline (up to 20 wt.%) and nepheline (approx. 10 wt.%), the latter being partly- to- significantly-replaced by natrolite (10-35 wt.%). Fine- to- medium-grained aegirine (15-20 wt.%) occurs as subhedral- to- anhedral, needle or columnar-shaped crystals, which commonly exhibit irregular rims and/or replacement textures of darker BSE contrast (Fig. 5c). Fine- to- medium-grained EGM (approx. 15 wt.%), can be concentrated in hinge zones of folds and be partly enriched in mm-wide bands, mainly composed of feldspar and clinopyroxene (Fig. 4c). In these bands elongated minerals are aligned while coarser-grained minerals form σ- and/or δ-clasts.

196 Eudialyte-group minerals are commonly elongated and ductile deformed in the direction of
197 foliation (Figs 3a, 4a and 6c). The crystals show no zoning or overgrowth textures but are
198 commonly intergrown with fine-grained, anhedral catapleiite and minor britholite-group
199 minerals. The most common accessories include galena and sphalerite.

200

201 Mid subunit (pegmatite-bearing aegirine meta-nepheline syenite)

202

203 This subunit contains variable amounts of leucocratic, mid- to coarse-grained and partly-
204 pegmatitic nepheline syenite schlieren (up to ten cm in thickness) set in a fine-grained
205 aegirine meta-nepheline syenite matrix. The dark green-grey matrix (grain size < 1mm) is
206 characterized by a homogeneous mineral distribution with no specific accumulation of
207 minerals (Fig. 3d). Deformation is displayed by the alignment of most of the mineral grains
208 (Fig. 4e) and stretching of rarely occurring larger crystals (e.g. catapleiite needles). The main
209 rock-forming minerals are anhedral albite (55 wt.%), nepheline (10 wt.%) and clinopyroxene
210 (20 wt.%) with minor microcline (5 wt.%), catapleiite (3 wt.%), EGM (2 wt.%), natrolite (3
211 wt.%) and accessory britholite- and rinkite-group minerals (≤ 0.25 wt.%). The latter are
212 always spatially associated with EGM.

213 The schlieren (Figs 3e-h and 4i-k) generally follow the foliation and the folding of the
214 rock. However, they also may be intercalated with the fine-grained matrix. The following
215 types of schlieren can be distinguished:

216 (A) Fine- to- medium-grained schlieren with no alignment of crystals, mainly
217 consisting of feldspar, clinopyroxene, euhedral to subhedral EGM and nepheline (e.g. Figs 3f
218 and h, 4i, 6a and b and 7d and e). In general, the relative content of clinopyroxene increases

219 towards the rims of these schlieren. Eudialyte-group minerals are medium- to- coarse-grained
220 reaching several mm in size (Figs 3f and h, 4k and 6a and b). Larger crystals are commonly
221 sector- or oscillatory-zoned. Porous and irregular zones in the central parts of euhedral
222 crystals can be complexly overgrown by areas with lower BSE contrast and along the rims of
223 such crystals flame textures with higher BSE contrast may be present (Figs 4k and6a and b).
224 Rims and cracks are commonly associated with catapleiite and britholite-group minerals,
225 occurring as filling of interstitial spaces or replacing EGM (Fig. 6a and b). Catapleiite occurs
226 as two textural varieties, (1) catapleiite spatially associated or intergrown with EGM,
227 preferably occurring at the border area between clinopyroxene and EGM (Fig. 7e) and (2)
228 catapleiite inclusions in fan-shaped sectors of radiating clinopyroxene aggregates (Figs 4i and
229 7d). These radial aggregates of subhedral clinopyroxenes (Fig. 7d) are unique to this schlieren
230 type. They are irregularly rimmed by areas with darker BSE contrast.

231 (B) Medium- to- coarse-grained schlieren with no general alignment of crystals. They
232 are mainly composed of subhedral- to- euhedral feldspar, nepheline, clinopyroxene and EGM
233 (Figs 3e and g, 4j, 5a and b and 7c). Euhedral- to subhedral eudialyte-group minerals mainly
234 exhibit sector zoning. Similar to schlieren (A) these are overgrown and/or replaced by
235 irregular or flamy areas with brighter BSE contrast (Fig. 4k). In cases EGM are extensively
236 altered and replaced by catapleiite and britholite-group minerals (Fig. 3g). In contrast to
237 schlieren (A), catapleiite is not necessarily spatially associated with EGM or clinopyroxene. It
238 may form needles, laths (rarely with a bluish color in hand specimen) or subhedral crystals
239 (Figs 3e and 7b). Clinopyroxene forms euhedral, coarse-grained and oscillatory- and/or
240 sector-zoned crystals (Fig. 5a and b). An exceptionally large (> 1 cm) and euhedral
241 clinopyroxene crystal was observed in sample 5408 (Figs 5a and 7c). This crystal exhibits a
242 partly-resorbed Zr-rich core, surrounded by an area rich in anhedral catapleiite inclusions,
243 followed by well-developed Ti-rich sectors and late irregular rims of Al-rich aegirine.

In both schlieren types, large, patchy aggregates composed of numerous euhedral fine-grained clinopyroxene crystals (Fig. 3e and h) occur. Nepheline and feldspar are extensively altered to natrolite (Figs 3e-h and 4e and j).

Outer subunit (catapleiite-bearing aegirine meta-nepheline syenite)

Both, magmatic and metamorphic terminology is used to describe the textural appearance of this subunit, although the classification of some of the features is not clear. This will be further commented in the discussion section.

This unit is up to several hundred meters in width, is schistose and fine-grained- to-aphanitic with porphyroclastic textures (Figs 3c and 4f-h). The contact towards the surrounding host rocks is characterized by an intense bleaching zone. Mineralogically, this rock type is very similar to the matrix of the mid subunit described above (Table 2), but is characterized by the absence of schlieren. Characteristic for this unit are medium-grained feldspars that form σ- and/or δ-clasts (Fig. 4f) as well as distinct EGM and catapleiite textures: In addition to fine-grained EGM in the matrix, larger poikilitic EGM porphyroclasts (Figs 3c, 4h and 6d) with abundant catapleiite (Figs 4h and 6d, Zr map), feldspar, nepheline and clinopyroxene inclusions occur, commonly surrounded by columnar rinkite-group minerals (Figs 4h and 6d). Furthermore, EGM in the outermost bleaching zones are partly- to-entirely replaced by zircon. Catapleiite forms up to 2 cm large, porphyroclasts (Fig. 4g) as well as elongated aggregates composed of anhedral, recrystallized catapleiite crystals (Fig. 7f). Clinopyroxene occurs as fine-grained euhedral- to- anhedral crystals rimed by a later clinopyroxene generation.

Other rock units

Arfvedsonite-aegirine meta-nepheline syenite (a.k.a. lakarpite)

Although being only a minor rock type restricted to the eastern contact of the mid subunit with the outer subunit (Fig. 2), this rock type is best known from the so-called *"discovery* outcrop*"* of the complex (Sjöqvist et al., 2013). This fine- to medium-grained unit mainly consists of feldspar (35-60 wt.%), arfvedsonite (up to 20 wt.%), clinopyroxene (up to 15 wt.%) and EGM (up to 12 wt.%) with minor nepheline and natrolite. Feldspar-rich schlieren contain cm-sized, pinkish and mostly poikilitic EGM commonly surrounded by an amphibole- and clinopyroxene-rich matrix. Clinopyroxene forms elongated to euhedral crystals, most other minerals are anhedral- to- subhedral in their habit.

Fluoro-leakeite-aegirine meta-nepheline syenite (a.k.a. kaxtorpite)

This fine- to- medium-grained rock with dark green- to- black colour was first described by Adamsson (1944) and is located in the very centre of the intrusion (Fig. 2). The rock is variably deformed showing alignment of elongated minerals culminating in intense isoclinal folding and crenulated foliation (Fig. 4d). Most minerals are anhedral, elongated and aligned forming small alternating bands. The fine-grained matrix consists of albite, fluoro-leakeite (Oberti et al., 2015), pectolite, clinopyroxene, nepheline and natrolite (± catapleiite, titanite,

fluorite and rosenbuschite) with large microcline augen preserved. The rock is commonly interfolded with the surrounding inner subunit.

Aegirine-amphibole-biotite meta-nepheline syenite (a.k.a. pulaskite)

This rock is only present in the western and northern part of the complex, mostly forming elongated bodies in the outer subunit (catapleiite-bearing aegirine meta-nepheline syenite; Fig. 2). This unit is dark bluish and fine- to- coarse-grained with white- to- colourless feldspar schlieren and contains boudin-shaped pods (up to decimetre size) of mafic rocks not yet investigated in detail. The rock consists of large and anhedral microcline crystals embedded or engulfed in fine- to medium-grained bands consisting of albite, clinopyroxene, biotite, amphibole ± fluorite. Most of these minerals are aligned, elongated and anhedral, only clinopyroxene and amphibole form euhedral crystals.

MINERAL COMPOSITIONS

Analytical techniques

Drill core samples were collected along two drill sections (J and P, nomenclature by Tasman Metals) at different depths of the intrusion (Fig. 2b and c). The investigated samples were selected to represent different styles of mineralization and degrees of alteration. Polished thick sections (120 µm) have been used for all analyses and a list of analyzed samples is given in Table 1.

Carbon-coated thick sections were studied by SEM-based Mineral Liberation Analyzer (MLA) and an Electron Probe Microanalyzer (EPMA) at the Helmholtz-Institute Freiberg for Resource Technology. The MLA studies used an FEI MLA Quanta 650F scanning electron microscope equipped with a field emission gun and two energy dispersive X-ray spectrometers (Bruker AXS Xflash® 5010) combined with image analysis software (Fandrich et al., 2007). Grain-based X-ray mapping (GXMAP) with resolution 500 x 500 pixels by a pixel size of 2µm with 5 pixel step size was applied at an acceleration voltage of 25 kV and a spot size of 5. The data was classified using the software package MLA Suite 3.0.

Electron Probe Microanalyzer measurements were performed with a JEOL JXA 8530F equipped with a field emission electron gun and five wavelength-dispersive spectrometers (WDS). Two of these spectrometers are provided with H-type crystals for high sensitivity and one with L-type crystals for good energy resolution. The X-ray element distribution maps were acquired with an acceleration voltage of 20 kV, a beam current of 50 nA, beam diameter of 14 µm and a dwell time of 140 ms. Aluminum, Y, Cl, and Ce were measured using the WDS, while Si, K, Ca, Mn, Zr, and Fe were measured with an energy dispersive spectrometer (EDS). Quantitative analyses of EGM were performed at an accelerating voltage of 20 kV and a beam current of 20 nA applying scanning mode as further details are described in Atanasova et al. (2015). Clinopyroxene, catapleiite, feldspar, nepheline and natrolite single point analyses were conducted at an accelerating voltage of 20 kV and a beam current of 20 nA. All further details are given in Electronic Appendix 2. Only aggregated analytical results are reported in Tables 3-7 and in Electronic Appendix 3. All detailed data is available on request by the senior author.

Clinopyroxene

Structural formula calculations for clinopyroxene are based on 4 cations and 6 oxygens, assuming stoichiometry. Average clinopyroxene analyses are given in Table 3. For classification we used the International Mineralogical Association (IMA/CNMMN) nomenclature (Morimoto et al., 1988; Rock, 1990) applying the classification diagram Jadeite (Jd) – Aegirine (Ae) – Quad (Q) with Quad (Q) being the sum of Ca-Mg-Fe pyroxene components (enstatite, ferrosilite, diopside and hedenbergite)

In the investigated samples, clinopyroxene is invariably sodic with a compositional range of $Jd_{2-40}Ae_{45-98}Q_{0-18}$ (Table 3, Fig. 8). Based on their textural appearance (see above), we distinguish the following five varieties, showing distinct compositions in an aegirine – (Ti+Zr)aegirine – jadeite ternary (Fig. 5).

(1) Resorbed cores (Fig. 5a) of zirconian aegirine (Zr-Ae) with compositions of Ae_{68-75}Ti/Zr-$Ae_{14-16}Jd_{3-4}$ featuring high Zr (up to 0.06 apfu) but low Ti (<0.02 apfu) contents.

(2) Clinopyroxene areas containing anhedral catapleiite inclusions (Fig. 5a), having compositions of Ae_{77-88}Ti/Zr-$Ae_{2-7}Jd_{4-10}$ with low Zr and Ti (<0.01 apfu) contents.

(3) Subhedral to anhedral, needle- or columnar-shaped clinopyroxene (Fig. 5c) exhibiting compositions of Ae_{76-88}Ti/Zr-$Ae_{1-6}Jd_{5-14}$. Most of these data fall into the field for aegirine (sensu stricto) with Ae ≥ 80, some of the data indicate calcian aegirine (Q ≥10) and a notable number of analyzes represent aluminian aegirine (Jd >10; Fig. 8).

(4) Titanian aegirine (Ti-Ae) with compositions of Ae_{67-87}Ti/Zr-$Ae_{3-15}Jd_{6-12}$ exhibiting low Zr (up to 0.03 apfu) but high Ti (up to 0.06 apfu) occurring as well-defined sectors and irregular areas. (Fig. 5a-c).

(5) Aluminian aegirine (Al-Ae) with compositions of $Ae_{56-75}Ti/Zr\text{-}Ae_{1-5}Jd_{17-35}$ forming anhedral rims (Fig. 5a-c) and/or irregular patchy areas crosscutting clinopyroxene types (3) and (4).

The frequency of the different clinopyroxene types varies strongly throughout the complex: In the mid subunit (1)-(5) occur, but in samples from the inner and the outer subunits (1) and (2) are absent, while (4) is rarely present. While (3) and (5) occur in similar amounts in the inner unit, in the outer unit (5) predominates over (3) (Fig. 5d).

The various clinopyroxene types are not only observed in the different subunits, but in single crystals too. As illustrated for samples 7315 and 6105 (Fig. 5b and c) from the inner unit, clinopyroxene (3) is anhedrally overgrown by (5). All five above-defined clinopyroxene types are present in a single crystal from the coarse-grained, undeformed schlieren (type B) of the mid subunit (sample 5408; Fig. 5a). Here, a Zr-aegirine core (1) is irregularly overgrown by aegirine (2) containing numerous anhedral catapleiite inclusions. Titanian-aegirine sectors (4) and aegirine (3) overgrow this most central part of the crystal. Aluminian-aegirine (5) anhedrally rims the crystal.

Eudialyte-group minerals

Formula calculations for EGM were carried out by normalizing the sum of (Si + Zr + Ti + Nb + Al + Hf) to 29 apfu (see details in Pfaff et al., 2010). In total 91 EGM grains from 13 samples were analyzed. The compiled data for each sample including an average for the particular units is given in Electronic Appendix 3.

379 The textural and compositional diversity of EGM analyzed is illustrated in Table 4 and
380 Figs 3, 6 and 9. In common with clinopyroxene, four textural varieties of EGM, which show
381 clear compositional differences are distinguished (Figs 6 and 9):

382 (1) Sector-zoned EGM enriched in Zr and depleted in REE and Nb.

383 (2) Oscillatory-zoned EGM that overgrow EGM (1); slightly enriched in Ca, Fe and
384 Cl, but depleted in REE.

385 (3) Irregular, up to several tens of micrometers wide areas with bright BSE contrast,
386 which replace and/or infiltrate EGM (1) and (2) (Fig. 4k). These are enriched in LREE and
387 show highest #Mn and ∑REE.

388 (4) Few micrometers wide rims or areas around vugs and/or cracks being enriched in
389 Y, HREE and #Mn, depleted in LREE with the highest ∑REEY and Nb.

390 In a given sample, sector and oscillatory-zoned EGM (1) and (2) are comparably REE-
391 poor and exhibit low #Mn (defined as Mn/(Fe+Mn)), whereas types (3) and (4) are REE-rich
392 and exhibit higher #Mn (Figs 6 and 9).

393 The most significant textural and compositional complexity is observed for EGM from
394 schlieren of the mid subunit, as was the case for clinopyroxene (see above). Sector-zoned
395 EGM (1) is observed in samples 7308 and 5618 (Figs. 6a and b), where sectors with high BSE
396 contrast are richer in Zr, REE and Y compared to sectors with low BSE contrast. These most
397 central parts of the crystals are overgrown either by oscillatory-zoned EGM (2) with
398 comparably higher Si, Ca, MREE and HREE but low LREE (Fig. 6b) or by irregular shaped
399 areas of type (3) with very high BSE contrast being enriched in REE and Y. Higher Y
400 contents are documented at the rim of the crystals as well as in poikilitic areas of type (4).

EGM type (3) mainly occurs in the inner subunit. These are fine-grained, deformed and texturally less complex crystals with no significant compositional variation (Fig. 6c). They coexist with clinopyroxene types (3) and (5) (Fig. 5c) and have the highest LREE and Mn enrichments (Fig. 9). EGM in the outer subunit are fine-grained of types (1) and (2) or poikilitic type (4) (Fig. 6d). Poikilitic EGM have the lowest LREE content compared to all EGM studied and show a particular depletion of REE at the rims (Fig. 6d, BSE and Ce map).

Furthermore, regional compositional differences in EGM compositions exist for Ca, Na, Y and the ΣHREE, where a general decrease from the outer to the inner subunit is present (Fig. 9). The opposite trend is noted for #Mn, ΣREE and ΣLREE, which increase from the border to the centre of the intrusion (Fig. 9). Niobium (apfu) and Zr/Hf ratios however, do not show such systematic changes, and Cl contents are mostly relatively low ($Cl_{apfu} < 0.5$), with one sample containing exceptionally Cl-rich EGM. These observations are in accordance with observations made by Sjöqvist et al. (2013).

Catapleiite

Structural formula calculations for catapleiite are based on 10 cations and 11 oxygens, assuming stoichiometry. Representative compositions are given in Table 5 and Fig. 7a. Catapleiites from two samples of the mid subunit were analyzed. In sample 5408 both textural varieties of Ca-catapleiite, namely coarse-grained subhedral crystals (Fig. 7b) and fine-grained anhedral inclusions in clinopyroxene (Fig. 7c) have very similar compositions with up to 7 wt.% CaO (Table 5). Similarly, in sample 5618 catapleiite occurrences at the border area between clinopyroxene and EGM and catapleiite inclusions in clinopyroxene (Fig. 7d and e)

424 exhibit quite similar compositions with CaO = 0.3-1.3 wt.% and Na_2O = 13.0-14.0 wt.%
425 (Table 5).

426

427 **Feldspars, feldspathoids and zeolithes**

428

429 Feldspars occur in all investigated samples as distinct albite and microcline grains and no
430 perthitic exsolution textures were observed. There are no significant differences between the
431 various samples and units with albite being almost pure (< 1 mol.% microcline) and
432 microcline containing up to 5 mol.% albite (Table 6).

433 Nepheline compositions ($Ne_{74-77}Ks_{21-25}An_0Qz_{0-1}$) in all samples are very similar (Table
434 7). According to the diagram after Hamilton (1961), the majority of analyses plot between the
435 ideal compositions of Morosewicz (M) and Buerger (B) (Fig. 10) and generally fall below the
436 isotherm at T = 700ºC, with two exceptional analyses indicating T > 775ºC.

437 Albite and nepheline are variably replaced by zeolithes. Natrolite is largely dominant
438 and shows a very restricted compositional variation. Analcime was found only in one sample
439 (Table 7).

440

441 **DISCUSSION**

442 The aim of this study is to distinguish the magmatic signature of an agpaitic complex from
443 features related to subsequent deformation and metamorphism using mineral textures and
444 compositions. In the course of the study, minerals of the feldspar-group and nepheline were
445 proven less beneficial probably due to their relatively simple structure and composition. In

446 contrast, structurally and compositionally more complex minerals of the eudialyte-group,
447 catapleiite as well as clinopyroxene appeared more appropriate to reflect physico-chemical
448 changes.

449

450 **Discrimination between magmatic and metamorphic features**

451 The agpaitic Norra Kärr complex was subsequently overprinted and deformed during two
452 successive orogenic events and is now preserved in a well-defined syncline with near parallel
453 occurrence of major rock units (Fig. 2b und c). In the following we assign the various textures
454 and compositions of the rock forming minerals to either magmatic relics or metamorphic
455 features in order to reconstruct the magmatic and the subsequent metamorphic history of the
456 Norra Kärr rocks.

457

458 Preserved magmatic features

459

460 Feldspars from the Norra Kärr rocks do not exhibit perthite or antiperthite textures preserved
461 (in agreement with Adamson 1944). We take this as evidence for the crystallization from a
462 subsolvus (low T) syenite (Sood & Edgar, 1970; Larsen & Sørensen, 1987; Markl, 2001;
463 Markl & Baumgartner, 2002; Chakrabarty et al., 2016). Alternatively, this could also reflect
464 the metamorphic recrystallization, but considering the observation that even feldspar
465 inclusions in EGM and clinopyroxene represent near end member compositions, a primary
466 subsolvus origin is considered most probable. This hypothesis is further supported by
467 temperatures derived from nepheline compositions, which generally do not exceed 700ºC
468 (Fig. 10). The two exceptional nepheline compositions that indicate T > 775 °C might
469 represent early magmatic (phenocrystic) relict nepheline.

Relics of an early magmatic crystallization stage of the Norra Kärr rocks might be represented by the Zr-aegrine cores of clinopyroxene (1) (Figs 5a and 7c). At constant P and T, Zr-aegirine is stable at moderate a_{Nds} (activity of $Na_2Si_2O_5$) and under relatively reducing conditions (Andersen et al., 2012). At this stage clinopyroxene could act as asink for Zr, preventing the crystallisation of early magmatic Zr-silicates. Similar relic clinopyroxene crystals were reported from the deformed Red Wine intrusion (Currie & Curtis, 1976), resulting from the large stabilitiy field of clinopyroxene and its ability to adapt its composition to the prevailing P-T-X conditions.

Subsequent destabilization of Zr-aegirine (Fig. 7c and d) results in the exsolution of catapleiite and Zr-poor clinopyroxene (2). The catapleiite inclusions occur in well-defined areas in clinopyroxene and are characterized by irregular shapes (Figs 5a and 7c). This process happened probably due to an increase of a_{Nds}, a_{H2O} or f_{O2} during a later crystallization stage and can be described by the schematic reaction:

$$4Na[Zr_{0.5}\,Fe_{0.5}]Si_2O_6\ (\text{Zr-Aegirine}) + Na_2Si_2O_5 + \tfrac{1}{2}O_2 + 4H_2O =$$
$$2NaFeSi_2O_6\ (\text{Aegirine}) + 2Na_2ZrSi_3O_9 * 2H_2O\ (\text{Catapleiite}) \qquad (1)$$

This hypothesis was tested by reintegrating the Zr-aegirine composition, using the molar volumes of catapleite inclusions contained in well-defined areas of aegirine (2) (Fig. 7d) as well as measured mineral compositions (Tables 3 and 5). Reintegrated Zr-aegirine compositions correspond very well with measured compositions (Table 8) supporting the argument for catapleiite formation by Zr-aegirine destabilization and subsequent exsolution. Considering the textural relationships illustrated in Fig. 7e, we assume that further catapleiite crystallized prior to EGM, forming euhedral crystals, which were later encased in EGM. In contrast, the textural relationships illustrated in Fig. 7d provide evidence that both minerals

495 may have replaced each other. In addition, it is not clear if the above-described catapleite
496 exsolutions in clinopyroxene and coarse, euhedral catapleite intergrown with EGM represent
497 different stages during the magmatic evolution of these rocks. Indeed, they may be two
498 different generations. Compositionally, however, there are no differences between these two
499 types of catapleiite (Fig. 7a). In general, both catapleiite and EGM occur in Zr-rich
500 peralkaline magmatic systems. However, the formation of magmatic EGM seems to require
501 relatively low water activities, but high Cl activities, conditions that are typically met in
502 reduced nepheline syenitic systems, whereas magmatic catapleiite seems to be restricted to
503 peralkaline (granitic) systems being relatively H_2O-rich (e.g., Andersen et al. 2010; Marks et
504 al., 2011; Andersen & Friis, 2015). Note that catapleiite can also form (along with many other
505 phases) during the hydrothermal alteration of EGM (e.g., Salvi et al., 2000; Karup-Møller et
506 al., 2010; Karup-Møller & Rose-Hansen, 2013; Borst et al., 2016). The catapleiite-eudialyte
507 equilibrium can be expressed by the following schematic reaction:

508

509 $3Na_2ZrSi_3O_9$ (Catapleiite) * $2H_2O + 6CaO + 4Na_2O + NaCl + 3FeO + 17SiO_2 =$

510 $Na_{15}Ca_6Fe_3Zr_3Si_{26}O_{72}(OH)_4Cl$ (Eudialyte) + $4H_2O$ (2).

511

512 The Cl contents in EGM from the Norra Kärr rocks mostly vary between 0.2-0.4 apfu
513 (Fig. 9a) and are relatively low compared to EGM in other alkaline complexes with Cl_{apfu} up
514 to 1.9 (see Schilling et al., 2011b). EGM from Norra Kärr may contain up to about 3 wt.%
515 H_2O (Atanasova et al., 2015). This implies that EGM may be stable even at relatively-low
516 a_{HCl} but relatively-high a_{H2O}. We propose that in the case of Norra Kärr a_{H2O} was not high
517 enough to stabilize catapleiite over a long crystallization interval. In addition, initial

518 catapleiite formation lead to subsequent REE enrichment of the melt, which probably was the
519 crucial promoting factor stabilizing EGM in this relatively Cl-poor environment.

520 On the deposit scale, we observe a continuous decrease in Ca, Na, Y and the HREE
521 with increasing #Mn, ΣREE and LREE from the outer to the inner subunit as demonstrated in
522 Fig. 9. Such compositional changes of EGM are attributed to primary magmatic evolution
523 (Sjöqvist et al., 2013) also known from EGM-bearing layered intrusions (e.g. Pfaff et al.,
524 2008; Schilling et al., 2011a; Sheard et al., 2012; Lindhuber et al., 2015; Ratschbacher et al.,
525 2015; Möller & Williams-Jones, 2016). These studies report compositional evolution in terms
526 of the Mn/(Fe+Mn) ratio and the content of the different REE, which is considered to be the
527 result of fractional crystallization during primary, magmatic layering of agpaitic intrusions
528 (Fig. 11). Early magmatic EGM are enriched in Fe and the HREE, which leads to subsequent
529 Mn- and- LREE-enrichment of the residual melt and to crystallization of late magmatic Mn-
530 and LREE-dominated EGM. Similarly, primary layering of the Norra Kärr complex (Fig. 11),
531 is indicated by early Fe- and- HREE-dominated EGM from the outer subunit as well as by
532 continuous Mn and LREE enrichment in the mid and inner subunits (Fig. 11) and are still
533 preserved within the fold structure.

534

535

536 Textures assigned to metamorphic overprint

537

538 The magmatic textures described above such as sector and oscillatory zoning in
539 clinopyroxene and EGM are partly-overgrown and/or replaced by late anhedral Al-aegirine
540 and REE-enriched EGM, respectively. The formation of Al-aegirine is a general feature of

541 metamorphosed syenites (Wooley et al., 1996) and is probably formed by the following
542 schematic reaction (Curtis & Gittins, 1979):

543

544 $NaAlSiO_4$ (Nepheline) + $NaAlSi_3O_8$ (Albite) = 2 $NaAlSi_2O_6$ (Jadeite) (3).

545

546 Same reaction is observed in samples studies from Norra Kärr as well. According to
547 (Curtis & Gittins, 1979) equation (3) could take place in a huge P- and- T-range of conditions,
548 between 450-700°C and 2-10 kbar, covering both, higher greenshist and lower- to- moderate
549 amphibolite facies conditions. In contrast to Red Wine, where amphibolite facies conditions
550 are reported, at Norra Kärr moderate- to- high greenshist facies conditions are only roughly
551 estimates. These estimates are supported by the observation that relic magmatic textures are
552 preserved due to assumed relatively low P and T during deformation of the rocks (Wooley et
553 al., 1996).

554 In EGM, flamy BSE textures (Figs 4k, 6a and b) as well as very late Y enrichments
555 and LREE depletions at the rim of crystals, along cracks, vugs (Figs 6a, b and d) and in highly
556 poikilitic areas (Figs 6b and d) are observed. Flamy textures as shown in Fig. 4k indicate
557 both, new formation of compositionally different EGM of type 3, (straight boundaries
558 between EGM (1) and (3)) as well as recrystallization or replacement of EGM types (1)
559 and/or (2) by EGM of type (3) (flamy EGM (3) permeating EGM (1) and/or (2)). Both can be
560 explained by the interaction with fluids, presumably generated during the metamorphic
561 overprint of the rocks. Yttrium and HREE enrichments accompanied by LREE depletion at
562 the rims of crystals (Fig. 6a, b and d) might document an even later event causing further
563 compositional adaptation of EGM, in this case accompanied by the re-distribution of REE and
564 Y, spatially-associated with the formation of late catapleiite and secondary LREE-rich

565 minerals (Fig. 6a, Ce map). We suggest that these textures could potentially be caused by
566 recrystallization of EGM in response to metamorphic deformation.

567 The widespread alteration of albite and nepheline to natrolite (Fig. 3) is also a late
568 process, probably related to fluid-assisted overprint during deformation. Importantly,
569 analcime is only very rarely observed (actually in only one sample, see above). This
570 corresponds to observations from the Mont Saint-Hilaire complex and Shushina Hill
571 (Schilling et al., 2011a; Chakrabarty et al., 2016, respectively) and it was suggested that
572 under such conditions analcime is only stable at low T < 150°C. Accordingly, this argues for
573 higher temperatures for natrolite formation. In the case of Norra Kärr a further indication for
574 the "metamorphic" origin is given by the spatial distribution of natrolite alteration, which
575 preferably occurs in the mid and inner units, while the very fine-grained rocks from the outer
576 unit are less affected, although these rocks are in direct contact with the granitic country rock.

577

578 **Thermodynamic modelling to constrain the p-T-conditions**

579

580 The albite – nepheline – aegirine assemblage of the Norra Kärr rocks permit estimations of
581 temperature and silica activity at the assumed pressure of the magmatic stage (e.g. Mitchell &
582 Platt, 1978; Markl et al., 2001, Schilling et al., 2011a) and may shed light into the so far-
583 poorly constrained conditions during metamorphic overprint during the Sveconorvegian
584 (Grenvillian) orogeny. We performed thermodynamic calculations applying the GEOCALC
585 software of Berman et al. (1987) and Liebermann & Petrakakis (1990) with the database of
586 Berman (1988) using the following three schematic equilibria.

587

588 $NaAlSiO_4$ (Nepheline) + SiO_2 (liq) = $NaAlSi_2O_6$ (Jadeite) (4)

589

590 $NaAlSi_2O_6$ (Jadeite) + SiO_2 (liq) = $NaAlSi_3O_8$ (Albite) (5)

591

592 $NaAlSiO_4$ (Nepheline) + $2SiO_2$ (liq) = $NaAlSi_3O_8$ (Albite) (6)

593

594 End member activities were calculated using a one-site mixing model for nepheline
595 and applying the solution activity formulations of Green et al. (2007) and Holland & Powell
596 (2003) for clinopyroxene and feldspar, respectively.

597 Assuming typical emplacement pressures of 1-2 kbar for syenitic peralkaline
598 intrusions (e.g., Konnerup-Madsen & Rose-Hansen, 1982; Salvi et al., 2000) and using the
599 mean compositions of Zr-aegirine (1), which we interpret as early magmatic clinopyroxene
600 (see above), equilibrium conditions of 600 - 700°C at a_{SiO2} values of 0.5-0.6 are indicated
601 (Fig. 12a). Such conditions are consistent with estimations for other peralkaline complexes
602 and are in agreement with the absence of perthitic alkali feldspar (see above) and the
603 temperature estimates based on nepheline thermometry (Fig. 10). Compositions of
604 presumably late-magmatic aegirine (2) and (3) indicate equilibration to lower temperatures (<
605 450°C) and a_{SiO2} values of < 0.3 (Fig. 12a).

606 Taken together, we interpret these data as representing the magmatic evolution of the
607 Norra Kärr rocks, indicating a relatively low liquidus temperature of <700°C and a relatively
608 extensive crystallization interval down to temperatures < 400°C, which has been
609 demonstrated before, based on both field studies (Markl et al., 2001; Marks et al., 2003;
610 Marks & Markl, 2003) and experimental work (Piotrowski & Edgar, 1970; Sood & Edgar,
611 1970; Giehl et al., 2013; 2014).

612 To constrain the metamorphic conditions of the Norra Kärr rocks during the
613 Sveconorvegian orogeny, we used the mean compositions of Al-aegirine (clinopyroxene 4;

see above) computed at pressures of 2.5, 5 and 8 kbars to represent general greenshist as well as lower amphibolite facies conditions (Fig. 12b). The calculated equilibrium temperatures range from 350 to 650°C with a_{SiO2} values from 0.55 to 0.15, with both T and a_{SiO2} decreasing with decreasing pressure. Comparing these estimates with proposed moderate to high greenschist facies conditions, temperatures from 400-550°C at pressure of 5 kbar with an a_{SiO2} range between 0.25 and 0.4 are considered as most reasonable. These values are similar to those estimated for late magmatic conditions. This might indicate that a_{SiO2} during the metamorphic stage did not essentially change, suggesting that fluid-rock interaction during this stage was largely (locally) rock-buffered and that the responsible fluids were not especially SiO_2-rich, as there is no late-stage quartz formed as might be expected from fluids derived from granitic country rocks.

.

CONCLUSIONS

Even after metamorphic overprint and deformation, it remains possible to identify primary magmatic textures and compositions in EGM and clinopyroxene from peralkaline rocks and to find evidence for primary magmatic layering of the intrusion with continuous enrichment of REE, LREE and Mn from the outer to the inner subunit. The multi-stage evolution of such rocks can be reconstructed using clinopyroxene and EGM, as both minerals cover a large stability range (in term of P and T) and are able to adapt their composition to changing conditions, thereby recording the magmatic and metamorphic history of the complex.

The minerals investigated probably crystallized from a subsolvus syenite and crystallization took place during a relatively extensive temperature interval from about 700ºC to 450ºC with a correspondent decrease in a_{SiO2} from 0.6 to about 0.3. Initially, Zr-aegirine

638 crystallized at relatively low peralkalinity and reducing conditions. Due to an increase in a_{Nds}
639 and at moderate- to- high f_{O2} and a_{H2O}, Zr-aegirine was destabilized and crystallization
640 continued forming aegirine (2) of sensu stricto compositions and catapleiite as the main Zr-
641 bearing silicate mineral. Due to the absence of sodalite and the very early formation of
642 catapleiite, a_{HCl} further increased and REE and HFSE were enriched in the residual melt,
643 promoting EGM crystallization. Crystallization of EGM seems not necessarily restricted to
644 specific conditions, forming even at very low a_{HCl} and at relatively high a_{H2O}, but to the
645 availability of specific elements in the melt.

646 During the Sveconorvegian/Grenvillian orogeny, the Norra Kärr rocks were deformed
647 and folded at presumably moderate greenshist facies conditions (Fig. 12) and late EGM and
648 Al-aegirine formed at 400ºC - 550ºC and in a a_{SiO2} range of 0.25-0.4 at pressures not
649 exceeding 5 kbar. We suggest that during this deformation event EGM interacted with
650 metamorphic fluids, either changing its composition or being partly-destabilized to catapleiite
651 and secondary REE-bearing minerals. During the whole history of the complex, a_{SiO2} remains
652 very similar, indicating very little interaction with the surrounding granitic rocks. This
653 assumption is confirmed by the relatively-restricted occurrence of natrolite alteration,
654 preferably occupying the more central part of the intrusion.

655

656 **ACKNOWLEDGEMENTS**

657

658 Research for this study was supported by and benefited from numerous discussions with Max
659 Frenzel, Axel Sjöqvist, Johan Berg and Magnus Leijd. Bernhard Schulz assisted with the
660 classification of meta-nepheline syenites and Kai Bachmann performed the high resolution
661 BSE images. The authors are deeply grateful for their support. Furthermore, the authors are

indebted to Tasman Metals Ltd. for supporting field work, providing rock samples, geological maps and cross sections. The manuscript was improved by the reviews of Roger Mitchell and Stefano Salvi. Their comments and suggestions are greatly appreciated. The authors thank A. Skelton for the editorial handling.

REFERENCES

Åberg, G. (1988). Middle Proterozoic anorogenic magmatism in Sweden and worldwide. *Lithos* **21**, 279-289.

Åberg, G., Kornfält, K.-A. & Nord, A. G. (1985a). Further radiometric dating of the Karlshamn granite, south Sweden. *GFF* **107**, 197-202.

Åberg, G., Kornfält, K.-A. & Nord, A. G. (1985b). The Vånga granite, south Sweden-a complex granitic intrusion. *GFF* **107**, 153-159.

Åberg, G., Löfvendahl, R. & Levi, B. (1984). The Götemar granite—isotopic and geochemical evidence for a complex history of an anorogenic granite. *GFF* **106**, 327-333.

Adamson, O. J. (1944). The petrology of the Norra Kärr district: An occurrence of alkaline rocks in southern Sweden. *GFF* **66**, 113-255.

Andersen, T., Carr, P. & Erambert, M. (2012). Late-magmatic mineral assemblages with siderite and zirconian pyroxene and amphibole in the anorogenic Mt Gibraltar microsyenite, New South Wales, Australia, and their petrological implications. *Lithos* **151**, 46-56.

Andersen, T., Erambert, M., Larsen, A. & Selbekk, R. (2010). Petrology of nepheline syenite pegmatites in the Oslo Rift, Norway: Zirconium silicate mineral assemblages as indicators of alkalinity and volatile fugacity in mildly agpaitic magma. *Journal of Petrology* **51**, 2303-2325.

Andersen, T. & Friis, H. (2015). The transition from agpaitic to hyperagpaitic magmatic crystallization in the Ilímaussaq alkaline complex, South Greenland. *Journal of Petrology* **56**, 1343-1364.

Andersson, U. B., Rutanen, H., Johansson, Å., Mansfeld, J. & Rimša, A. (2007). Characterization of the Paleoproterozoic mantle beneath the Fennoscandian Shield: Geochemistry and isotope geology (Nd, Sr) of~ 1.8 Ga mafic plutonic rocks from the Transscandinavian Igneous Belt in southeast Sweden. *International Geology Review* **49**, 587-625.

Andréasson, P. G. & Rodhe, A. (1994). Ductile and brittle deformation within the Protogine Zone, southern Sweden: a discussion.

Arzamastsev, A., Bea, F., Glaznev, V., Arzamastseva, L. & Montero, P. (2001). Kola alkaline province in the Paleozoic: evaluation of primary mantle magma composition and magma generation conditions. *Russian Journal of Earth Sciences* **3**, 3-24.

Arzamastsev, A., Belyatsky, B., Travin, A., Arzamastseva, L. & Tsarev, S. (2005). Dike Rocks in the Khibina Massif: Relations with the Plutonic Series, Age, and Characteristics of the Mantle Source. *Petrology* **13**, 267-288.

Atanasova, P., Krause, J., Möckel, R., Osbahr, I. & Gutzmer, J. (2015). Electron Probe Microanalysis of REE in Eudialyte Group Minerals: Challenges and Solutions. *Microscopy and Microanalysis* **21**, 1096-1113.

Berman, R., Brown, T. & Perkins, E. (1987). GeO-calc–software for calculation and display of P–T–X phase diagrams. *American Mineralogist* **72**, 861-862.

Berman, R. G. (1988). Internally-consistent thermodynamic data for minerals in the system Na2O-K2O-CaO-MgO-FeO-Fe2O3-Al2O3-SiO2-TiO2-H2O-CO2. *Journal of Petrology* **29**, 445-522.

Bingen, B., Nordgulen, O. & Viola, G. (2008). A four-phase model for the Sveconorwegian orogeny, SW Scandinavia. *Norsk Geologisk Tidsskrift* **88**, 43.
Bingen, B., Stein, H. J., Bogaerts, M., Bolle, O. & Mansfeld, J. (2006). Molybdenite Re–Os dating constrains gravitational collapse of the Sveconorwegian orogen, SW Scandinavia. *Lithos* **87**, 328-346.
Borst, A. M., Friis, H., Andersen, T., Nielsen, T., Waight, T. E. & Smit, M. A. (2016). Zirconosilicates in the kakortokites of the Ilímaussaq complex, South Greenland: Implications for fluid evolution and high-field-strength and rare-earth element mineralization in agpaitic systems. *Mineralogical Magazine* **80**, 5-30.
Brander, L. (2011). *The Mesoproterozoic Hallandian event-a region-scale orogenic event in the Fennoscandian Shield*.
Brander, L. & Söderlund, U. (2009). Mesoproterozoic (1.47–1.44 Ga) orogenic magmatism in Fennoscandia; Baddeleyite U–Pb dating of a suite of massif-type anorthosite in S. Sweden. *International Journal of Earth Sciences* **98**, 499-516.
Breemen, O. v. & Currie, K. (2004). Geology and U Pb geochronology of the Kipawa Syenite Complex a thrust related alkaline pluton and adjacent rocks in the Grenville Province of western Quebec. *Canadian Journal of Earth Sciences* **41**, 431-455.
Chakrabarty, A., Mitchell, R., Ren, M., Saha, P., Pal, S., Pruseth, K. & Sen, A. (2016a). Magmatic, hydrothermal and subsolidus evolution of the agpaitic nepheline syenites of the Sushina Hill Complex, India: implications for the metamorphism of peralkaline syenites. *Mineralogical Magazine* **80**, 1161-1193.
Chakrabarty, A., Pruseth, K. L. & Sen, A. K. (2012). Compositions and petrogenetic significance of the eudialyte group minerals from Sushina, Purulia, West Bengal. *Journal of the Geological Society of India* **79**, 449-459.
Currie, K. & Curtis, L. (1976). An application of multicomponent solution theory to jadeitic pyroxenes. *The Journal of Geology*, 179-194.
Currie, K. L. & Breemen, O. v. (1996). The Origin of Rare Minerals in the Kipawa Syenite Complex Western Quebec. *The Canadian Mineralogist* **34**, 435-451.
Curtis, L. & Currie, K. L. (1981). *Geology and petrology of the Red Wine alkaline complex, central Labrador*: Geological Survey of Canada.
Curtis, L. & Gittins, J. (1979). Aluminous and titaniferous clinopyroxenes from regionally metamorphosed agpaitic rocks in central Labrador. *Journal of Petrology* **20**, 165-186.
Dostal, J. (2015). Rare Metal Deposits Associated with Alkaline/Peralkaline Igneous Rocks. *Reviews in Economic Geology* **18**.
Fandrich, R., Gu, Y., Burrows, D. & Moeller, K. (2007). Modern SEM-based mineral liberation analysis. *International Journal of Mineral Processing* **84**, 310-320.
Giehl, C., Marks, M. & Nowak, M. (2013). Phase relations and liquid lines of descent of an iron-rich peralkaline phonolitic melt: an experimental study. *Contributions to Mineralogy and Petrology* **165**, 283-304.
Giehl, C., Marks, M. A. & Nowak, M. (2014). An experimental study on the influence of fluorine and chlorine on phase relations in peralkaline phonolitic melts. *Contributions to Mineralogy and Petrology* **167**, 1-21.
Gillespie, M. & Styles, M. (1999). BGS rock classification scheme, Volume 1. Classification of igneous rocks.
Goodenough, K. M., Schilling, J., Jonsson, E., Kalvig, P., Charles, N., Tuduri, J., Deady, E. A., Sadeghi, M., Schiellerup, H., Müller, A., Bertrand, G., Arvanitidis, N., Eliopoulos, D. G., Shaw, R. A., Thrane, K. & Keulen, N. (2016). Europe's rare earth element resource potential: An overview of REE metallogenetic provinces and their geodynamic setting. *Ore Geology Reviews* **72, Part 1**, 838-856.
Goswami, B. & Basu, S. K. (2013). Metamorphism of Proterozoic agpaitic nepheline syenite gneiss from North Singhbhum Mobile Belt, eastern India. *Mineralogy and Petrology* **107**, 517-538.
Green, E., Holland, T. & Powell, R. (2007). An order-disorder model for omphacitic pyroxenes in the system jadeite-diopsidehedenbergite-acmite, with applications to eclogitic rocks. *American Mineralogist* **92**, 1181-1189.

Hamilton, D. (1961). Nephelines as crystallization temperature indicators. *The Journal of Geology*, 321-329.
Högdahl, K., Andersson, U. B. & Eklund, O. (2004). *The Transscandinavian Igneous Belt (TIB) in Sweden: a review of its character and evolution*: Geological survey of Finland.
Holland, T. & Powell, R. (2003). Activity–composition relations for phases in petrological calculations: an asymmetric multicomponent formulation. *Contributions to Mineralogy and Petrology* **145**, 492-501.
Karup-Møller, S. & Rose-Hansen, J. (2013). New data on eudialyte decomposition minerals from kakortokites and associated pegmatites of the Ilímaussaq complex, South Greenland. *Geological Society of Denmark. Bulletin* **61**, 47-70.
Karup-Møller, S., Rose-Hansen, J. & Sørensen, H. (2010). Eudialyte decomposition minerals with new hitherto undescribed phases from the Ilímaussaq complex, South Greenland. *Geological Society of Denmark. Bulletin* **58**, 75-88.
Kogarko, L. (1987). Alkaline rocks of the eastern part of the Baltic Shield (Kola Peninsula). *Geological Society, London, Special Publications* **30**, 531-544.
Kogarko, L. (1990). Ore-forming potential of alkaline magmas. *Lithos* **26**, 167-175.
Kogarko, L., Lazutkina, L. & Romanchev, B. (1982). Problems of Genesis of Eudialyte Mineralization. *Geokhimiya*, 1415-1432.
Konnerup-Madsen, J. & Rose-Hansen, J. (1982). Volatiles associated with alkaline igneous rift activity: fluid inclusions in the Ilímaussaq intrusion and the Gardar granitic complexes (South Greenland). *Chemical Geology* **37**, 79-93.
Larsen, L. M. & Sørensen, H. (1987). The Ilímaussaq intrusion—progressive crystallization and formation of layering in an agpaitic magma. *Geological Society, London, Special Publications* **30**, 473-488.
Liebermann, J. & Petrakakis, K. (1991). TWEEQU Thermobarometry: Analysis of Uncertainties and Applications to Granulites from Western Alaska and Austria. *Canadian mineralogist* **29**, 857-887.
Lindhuber, M. J., Marks, M. A., Bons, P. D., Wenzel, T. & Markl, G. (2015). Crystal mat-formation as an igneous layering-forming process: Textural and geochemical evidence from the 'lower layered'nepheline syenite sequence of the Ilímaussaq complex, South Greenland. *Lithos* **224**, 295-309.
Markl, G. (2001). A new type of silicate liquid immiscibility in peralkaline nepheline syenites (lujavrites) of the Ilimaussaq complex, South Greenland. *Contributions to Mineralogy and Petrology* **141**, 458-472.
Markl, G. & Baumgartner, L. (2002). pH changes in peralkaline late-magmatic fluids. *Contributions to Mineralogy and Petrology* **144**, 331-346.
Markl, G., Marks, M., Schwinn, G. & Sommer, H. (2001). Phase equilibrium constraints on intensive crystallization parameters of the Ilímaussaq Complex, South Greenland. *Journal of Petrology* **42**, 2231-2257.
Marks, M. & Markl, G. (2003). Ilímaussaq 'en miniature': closed-system fractionation in an agpaitic dyke rock from the Gardar Province, South Greenland (contribution to the mineralogy of Ilímaussaq no. 117). *Mineralogical Magazine* **67**, 893-919.
Marks, M., Vennemann, T. W., Siebel, W. & Markl, G. (2003). Quantification of magmatic and hydrothermal processes in a peralkaline syenite–alkali granite complex based on textures, phase equilibria, and stable and radiogenic isotopes. *Journal of Petrology* **44**, 1247-1280.
Marks, M. A., Hettmann, K., Schilling, J., Frost, B. R. & Markl, G. (2011). The mineralogical diversity of alkaline igneous rocks: critical factors for the transition from miaskitic to agpaitic phase assemblages. *Journal of Petrology* **52**, 439-455.
Marks, M. A. & Markl, G. (2015). The Ilímaussaq alkaline complex, South Greenland. *Layered Intrusions*: Springer, 649-691.
McLelland, J. M. (1989). Crustal growth associated with anorogenic, mid-Proterozoic anorthosite massifs in northeastern North America. *Tectonophysics* **161**, 331-341.

Mitchell, R. H. (2015). Primary and secondary niobium mineral deposits associated with carbonatites. *Ore Geology Reviews* **64**, 626-641.
Mitchell, R. H. & Platt, R. G. (1978). Mafic mineralogy of ferroaugite syenite from the Coldwell alkaline complex, Ontario, Canada. *Journal of Petrology* **19**, 627-651.
Möller, V. & Williams-Jones, A. E. (2016). Petrogenesis of the Nechalacho Layered Suite, Canada: Magmatic Evolution of a REE–Nb-rich Nepheline Syenite Intrusion. *Journal of Petrology* **57**, 229-276.
Morimoto, N., Fabries, J., Ferguson, A., Ginzburg, I., Ross, M., Seifert, F., Zussman, J., Aoki, K. & Gottardi, G. (1988). Nomenclature of pyroxenes. *American Mineralogist* **73**, 1123-1133.
Nanda, J., Gupta, S. & Dobmeier, C. (2008). Metamorphism of the Koraput Alkaline Complex, Eastern Ghats Province, India—evidence for reworking of a granulite terrane. *Precambrian Research* **165**, 153-168.
Oberti, R., Boiocchi, M., Hawthorne, F. C., Ball, N. A. & Harlow, G. E. (2015). Eckermannite revised: The new holotype from the Jade Mine Tract, Myanmar—crystal structure, mineral data, and hints on the reasons for the rarity of eckermannite. *American Mineralogist* **100**, 909-914.
Pekov, I. (1998). Yttrium mineralization in the Khibiny–Lovozero alkaline complex (Kola Peninsula). *Zapiski VMO* **5**, 66-85.
Pfaff, K., Krumrei, T., Marks, M., Wenzel, T., Rudolf, T. & Markl, G. (2008). Chemical and physical evolution of the 'lower layered sequence'from the nepheline syenitic Ilímaussaq intrusion, South Greenland: Implications for the origin of magmatic layering in peralkaline felsic liquids. *Lithos* **106**, 280-296.
Pfaff, K., Wenzel, T., Schilling, J., Marks, M. A. & Markl, G. (2010). A fast and easy-to-use approach to cation site assignment for eudialyte-group minerals. *Neues Jahrbuch für Mineralogie-Abhandlungen: Journal of Mineralogy and Geochemistry* **187**, 69-81.
Piotrowski, J. M. & Edgar, A. D. (1970). Melting relations of undersaturated Alkaline rocks from south Greenland compared to those of Africa and Canada. *Meddelelser om Grönland* **181**, 1-62.
Rankin, L. (2011). Structural setting of the Norra Kärr intrusive complex, Central Sweden. Geointerp Confidential Report 2011/14.
Ratschbacher, B. C., Marks, M. A., Bons, P. D., Wenzel, T. & Markl, G. (2015). Emplacement and geochemical evolution of highly evolved syenites investigated by a combined structural and geochemical field study: The lujavrites of the Ilímaussaq complex, SW Greenland. *Lithos* **231**, 62-76.
Rock, N. (1990). The International Mineralogical Association (IMA/CNMMN) pyroxene nomenclature scheme: computerization and its consequences. *Mineralogy and Petrology* **43**, 99-119.
Salvi, S., Fontan, F., Monchoux, P., Williams-Jones, A. & Moine, B. (2000). Hydrothermal mobilization of high field strength elements in alkaline igneous systems: evidence from the Tamazeght Complex (Morocco). *Economic Geology* **95**, 559-576.
Schilling, J., Marks, M. A., Wenzel, T., Vennemann, T., Horváth, L., Tarassoff, P., Jacob, D. E. & Markl, G. (2011a). The magmatic to hydrothermal evolution of the intrusive mont saint-hilaire complex: Insights into the late-stage evolution of peralkaline rocks. *Journal of Petrology* **52**, 2147-2185.
Schilling, J., Wu, F.-Y., McCammon, C., Wenzel, T., Marks, M., Pfaff, K., Jacob, D. & Markl, G. (2011b). The compositional variability of eudialyte-group minerals. *Mineralogical Magazine* **75**, 87-115.
Sheard, E. R., Williams-Jones, A. E., Heiligmann, M., Pederson, C. & Trueman, D. L. (2012). Controls on the Concentration of Zirconium, Niobium, and the Rare Earth Elements in the Thor Lake Rare Metal Deposit, Northwest Territories, Canada. *Economic Geology* **107**, 81-104.
Sjöqvist, A. S. (2015). Agpaitic rocks of the Norra Kärr alkaline complex. *Earth Sciences*: University of Gothenburg, 42.
Sjöqvist, A. S., Cornell, D. H., Andersen, T., Andersson, U. B., Christensson, U. I., Ranjer, S. J., Holtstam, D. & Leijd, M. (2014). Geochronology of the Norra Kärr alkaline complex, southern Sweden. *31st Nordic Geological Winter Meeting, Lund, Sweden*.
Sjöqvist, A. S., Cornell, D. H., Andersen, T., Erambert, M., Ek, M. & Leijd, M. (2013). Three compositional varieties of rare-earth element ore: eudialyte-group minerals from the Norra Kärr Alkaline Complex, Southern Sweden. *Minerals* **3**, 94-120.

Smellie, J. A. & Stuckless, J. S. (1985). Element mobility studies of two drill-cores from the Goetemar Granite (Kraakemaala test site), Southeast Sweden. *Chemical Geology* **51**, 55-78.
Smith, M., Moore, K., Kavecsánszki, D., Finch, A., Kynicky, J. & Wall, F. (2016). From mantle to critical zone: A review of large and giant sized deposits of the rare earth elements. *Geoscience Frontiers*.
Söderlund, U., Patchett, P. J., Vervoort, J. D. & Isachsen, C. E. (2004). The 176 Lu decay constant determined by Lu–Hf and U–Pb isotope systematics of Precambrian mafic intrusions. *Earth and Planetary Science Letters* **219**, 311-324.
Sood, M. & Edgar, A. (1970). Melting Relations of Undersaturated Alkaline Rocks from the Ilímaussaq Intrusion and Grønnedal-Íka Complex, South Greenland. *Meddelelser om Grönland* **181**, 41.
Sørensen, H. (1960). *On the agpaitic rocks*: Grønlands geologiske undersøgelse.
Sørensen, H. (1997). The agpaitic rocks; an overview. *Mineralogical Magazine* **61**, 485-498.
Sørensen, H., Bohse, H. & Bailey, J. C. (2006). The origin and mode of emplacement of lujavrites in the Ilímaussaq alkaline complex, South Greenland. *Lithos* **91**, 286-300.
Tilley, C. E. (1954). Nepheline-alkali feldspar parageneses. *American Journal of Science* **252**, 65-75.
Törnebohm, A. E. (1906). Katapleiite-syenit, en nyupptäckt varietet af nefelinsyenit i Sverige. *SGU Series C*, 1-54.
Upton, B. G. (2013). Tectono-magmatic evolution of the younger Gardar southern rift, South Greenland. *Geological Survey of Denmark & Greenland Bulletin*.
Ussing, N. V. (1912). *Geology of the country around Julianehaab, Greenland*: I commission hos CA Reitzel.
von Eckermann, H. (1968). New contributions to the interpretation of the genesis of the Norra Kärr alkaline body in Southern Sweden. *Lithos* **1**, 76-88.
Wahlgren, C.-H., Cruden, A. R. & Stephens, M. B. (1994). Kinematics of a major fan-like structure in the eastern part of the Sveconorwegian orogen, Baltic Shield, south-central Sweden. *Precambrian Research* **70**, 67-91.
Wahlgren, C. & Stephens, M. (2004). Tectonometamorphic reworking of TIB rocks during the Sveconorwegian orogeny, south-central Sweden. *SPECIAL PAPER-GEOLOGICAL SURVEY OF FINLAND* **37**, 56.
Woolley, A. R., Platt, R. G. & Eby, G. N. (1996). Relatively Aluminous Alkali Pyroxene in Nepheline Syenite from Malawi. *The Canadian Mineralogist* **34**, 423-434.

Fig.1. (a) Simplified geological map of Fennoscandia illustrating major lithological units (modified after Högdahl et al., 2004). Red box is enlarged in (b), where the red ellipse resembles the Norra Kärr complex. The white arrow indicates the direction of decreasing regional deformation during the Sveconorwegian orogeny. PZ-Protogine Zone, SFDZ - Sveconorwegian Frontal Deformation Zone (simplified after Sönderlund et al., 2002; Wahlgren et al., 1994).

Fig.2. (a) Simplified geological map of the Norra Kärr complex illustrating major lithological units (modified after Tasman Metals Ltd). The deformation is well visualized in W-E cross sections (b) J and (c) P. The sampling locations as given in Table 1 are marked as black crosses.

Fig.3. Mineral Liberation Analyzer (MLA) classified-color images (EDX-GXMAP mode) of the different subunits of Norra Kärr. Illustrated are characteristic textures of a) the incipient alignment and stretching of minerals and b) the macroscopic scale folding and alignment of minerals in the inner subunit; (c) poikilitic EGM in a fine grained matrix of the outer subunit; (d) homogeneous matrix of the mid subunit; (e)-(h) thoroughly preserved euhedral to subhedral EGM and clinopyroxene in leucocratic schlieren of the mid subunit. Nepheline is partly to strongly altered to natrolite. Areas marked as red boxes are enlarged in Figs 4, 5 and 6.

Fig.4. (a) Alignment of minerals as well as (b) and (c) microscopic- to macroscopic scale folding as common features of the inner subunit; EGM crystals in (a) are slightly stretched. (d) Folding of the fluoro-leakeite-aegirine meta-nepheline syenite rock. (e) Fine-grained meta-nepheline syenite with a band of mid- to- coarse-grained nepheline and eudialyte. The nepheline crystals show alteration. (f) Microcline δ-clast, (g) catapleiite and (h) EGM (type (4)) porphyroclasts are characteristic for the outer subunit. EGM contain inclusions of catapleiite, feldspar, nepheline and clinopyroxene. Catapleiite (Cat) forms tails and replaces EGM mainly at the rim. EGM are surrounded by columnar rinkite-group minerals (Rink). (i) Medium-grained schlieren of the mid subunit with feldspar, aegirine and eudialyte show no particular alignment, aegirine crystals (CPX) form radiating aggregates. (i) Coarse-grained microcline and extensively altered nepheline from schlieren of the mid subunit. (k) EGM (3) overgrow and/or replace the compositionally different EGM (1) in schlieren of the mid subunit; visible white spots represent EPMA measurement locations.

Fig.5. Compositional and textural characteristics of clinopyroxene from the Norra Kärr rocks. (a) Euhedral clinopyroxene from the mid unit (sample 5408). The resorbed Zr-aegirine core is irregularly rimmed by aegirine s.s. rich in catapleiite inclusions. Both are overgrown by alternating sectors of inclusion-free titanoan-aegirine and aegirine s.s. Anhedral Al-aegirine rims irregularly the crystal. (b) Subhedral clinopyroxene from the mid subunit exhibiting well

defined Ti-rich sectors overgrown by Al-aegirine. In the center a large catapleiite is enclosed. (c) Subhedral to anhedral clinopyroxene of the inner subunit; (d) Anhedral clinopyroxene from the outer subunit. See also detailed descriptions in the main text.

Fig.6. Compositional and textural characteristics of EGM from the Norra Kärr rocks. At the top of the diagram, textural varieties 1-4 from all EGM investigated are collated considering the #Mn and the $REEY_{apfu}$. Representative grains of the different units are shown in (a)-(d). In the mid subunit (a) single EGM crystal (sample 5618) shows sectors (1) being Zr-rich, but REE-poor, overgrown by an irregular flamy area (3) of high BSE contrast, rich in REE and Y. Highest Y is detected along rims and cracks (4). The crystal is closely associated with catapleite (Cat) and britholite group minerals (Brit). Red box is enlarged in Fig. 4k. (b) Subhedral EGM featuring sector (1) and oscillatory (2) zoning, as well as irregular flamy textures (3) and poikilitic Y-rich areas (4). (c) EGM crystals from the inner subunit commonly show deformation features like stretching and alignment and are high in #Mn and REE. (d) Poikilitic EGM porphyroclast from the outer unit showing LREE depletion and Y enrichments at the rim. Catapleite (Cat) and rinkite group minerals (Rink) are visible as white areas in the Zr and Ce maps. Visible spots in (a) and (b) represent EPMA (white) and LA-ICP-MS (dark) measurement locations.

Fig.7. Compositional (a) and textural (b-f) characteristics of catapleite from the Norra Kärr rocks. (b) A single euhedral Ca-catapleiite crystal (Ca-Cat) and (c) Ca-catapleiite inclusions (Ca-Cat) in clinopyroxene, aegirine s.s. (CPX) (Fig. 4a) from schlieren of the mid subunit, sample 5408; (d) and (e) show characteristic catapleiite (Cat) and EGM textures in the mid subunit, sample 5618. Zones in radial aegirine s.s. (CPX), rich in catapleiite inclusions (Cat) are remarkably well defined. Catapleiite occurs enclosed in EGM, between and within EGM crystals and at the grain boundaries between clinopyroxene and EGM. (f) Catapleiite aggregates (Cat) from the outer subunit, sample 5611. Visible spots in (b) and (c) represent EPMA (white) and LA-ICP-MS (dark) measurement locations.

Fig.8. (a) Classification diagram for Ca-Na and Na pyroxenes with the endmembers Jadeite (Jd) – Aegirine (Ae) – Quad (Q) modified after Morimoto et al. (1988) and Rock (1990). The marked area is enlarged in (b) showing that pyroxene composiitons from Norra Kärr include aegirine s.s., zirconian aegirine, calcian aegirine, titanoan aegirine and aluminian aegirine.

Fig.9. Distribution of (a) major and (b) minor elements in EGM according to the relative sampling location within the fold structure. Samples from the discovery outcrop are displayed for comparison. Colour coding displays EGM textural varieties 1-4 as defined in Fig. 5.

Fig.10. Diagram of the system nepheline-kalsilite-silica (wt.%) with isotherms showing the limit of nepheline solid solution at the indicated temperatures (after Hamilton 1961). The majority of analyses plot within the Morosewicz (M) – Buerger (B) convergence field (after Tilley, 1954). Most of the analyses indicate $T \leq 500$ºC. Only two analyses indicate $T \geq 700$ºC.

Fig.11. Suggested primary magmatic layering of the intrusion with upwards enrichment of REE, LREE and #Mn, preserved within the present fold structure.

Fig.12. Two silica activity (a_{SiO2}) - temperature diagrams calculated based on equilibria (4)-(6). Different sets of conditions (different lines in (b)) are calculated due to variable activities of nepheline (aNe) and jadeite (aJd), while the activity of albite (aAb) is 1 for all reactions. (a) Magmatic conditions are estimated for 1-2 kbar using early- and late-magmatic clinopyroxene compositions, respectively. (b) The metamorphic evolution of the Norra Kärr complex is illustrated for pressures representing general greenshist (grey area) to lower amphibolite facies conditions, considering metamorphic clinopyroxene textures and compositions. Details are given in the main text.

Electronic Appendix 1. Selected scans of core samples. (a) Folded fluoro-leakeite-aegirine meta-nepheline syenite. (b) Catapleiite-and EGM-bearing aegirine meta-nepheline syenite with 5 % pegmatoidal schlieren shows folding of the rock. (c) Catapleiite-and EGM-bearing aegirine meta-nepheline syenite with 30 to 50 % pegmatoidal schlieren with small scale folding of the schlieren, minerals show hematization. (d) Foliated fine- to- medium-grained aegirine leuco-meta-nepheline syenite. (e) Coarse-grained schlieren with microcline, albite and EGM, fine-grained euhedral aegirines form patchy aggregates.

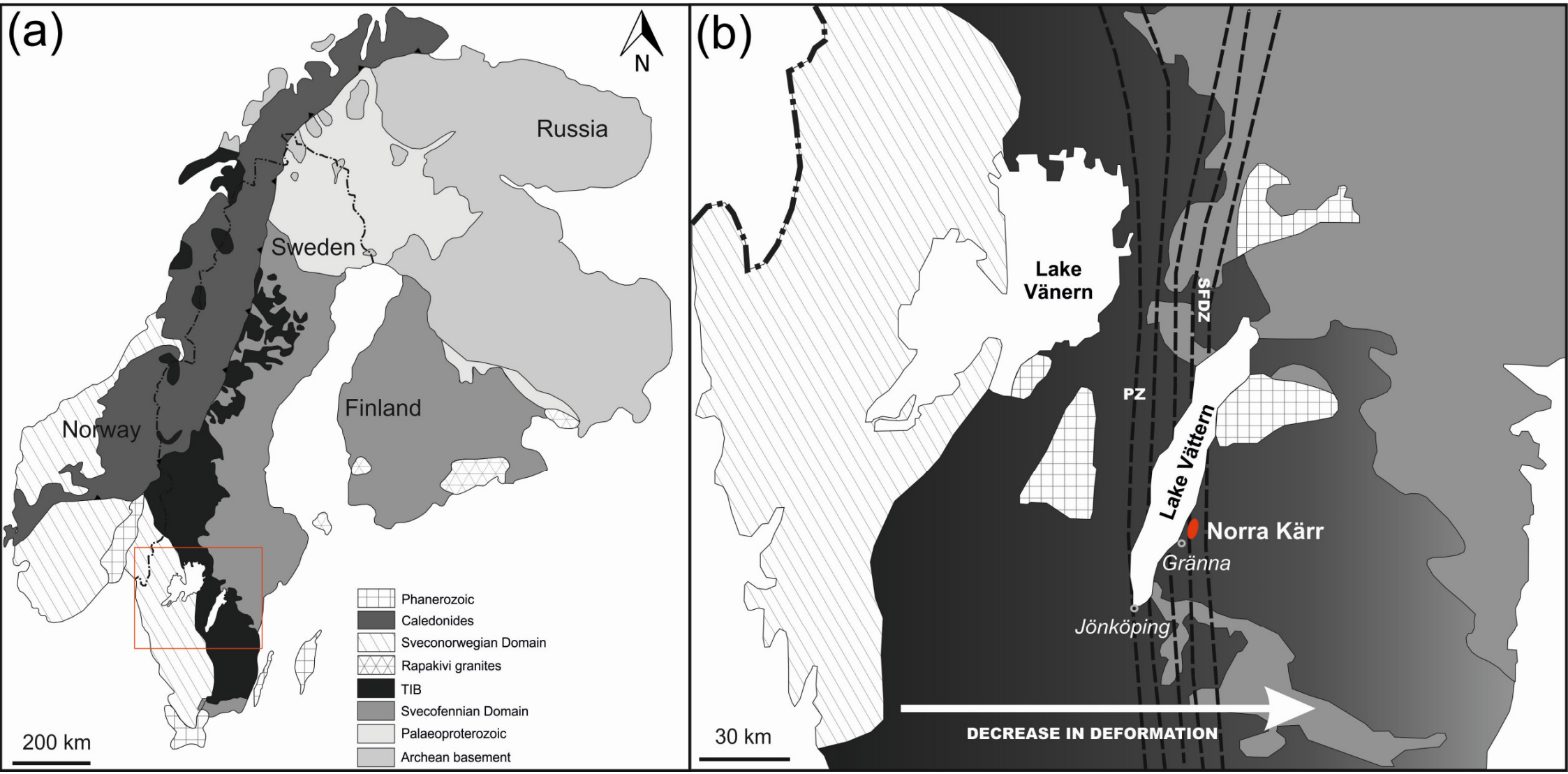
(a)
N
Russia
Sweden
Finland
Norway
Phanerozoic
Caledonides
Sveconorwegian Domain
Rapakivi granites
TIB
Svecofennian Domain
Palaeoproterozoic
Archean basement
200 km
(b)
Lake Vänern
SFDZ
PZ
Lake Vättern
Norra Kärr
Gränna
Jönköping
DECREASE IN DEFORMATION
30 km

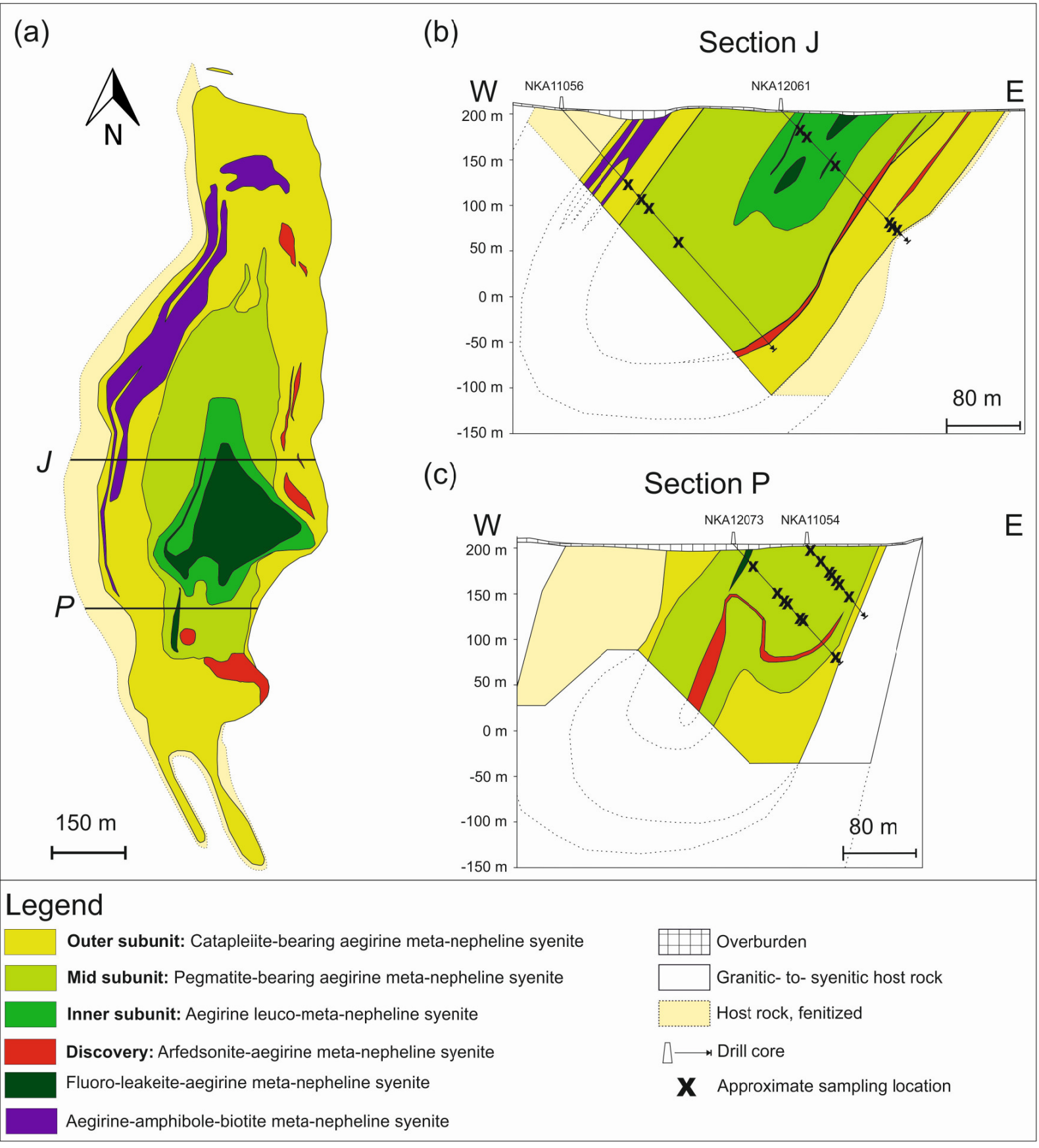
(a)
N
J
P
150 m
(b)
Section J
W
E
NKA11056
NKA12061
200 m
150 m
100 m
50 m
0 m
-50 m
-100 m
-150 m
80 m
(c)
Section P
W
E
NKA12073
NKA11054
200 m
150 m
100 m
50 m
0 m
-50 m
-100 m
-150 m
80 m
Legend
Outer subunit: Catapleiite-bearing aegirine meta-nepheline syenite
Mid subunit: Pegmatite-bearing aegirine meta-nepheline syenite
Inner subunit: Aegirine leuco-meta-nepheline syenite
Discovery: Arfedsonite-aegirine meta-nepheline syenite
Fluoro-leakeite-aegirine meta-nepheline syenite
Aegirine-amphibole-biotite meta-nepheline syenite
Overburden
Granitic- to- syenitic host rock
Host rock, fenitized
Drill core
Approximate sampling location

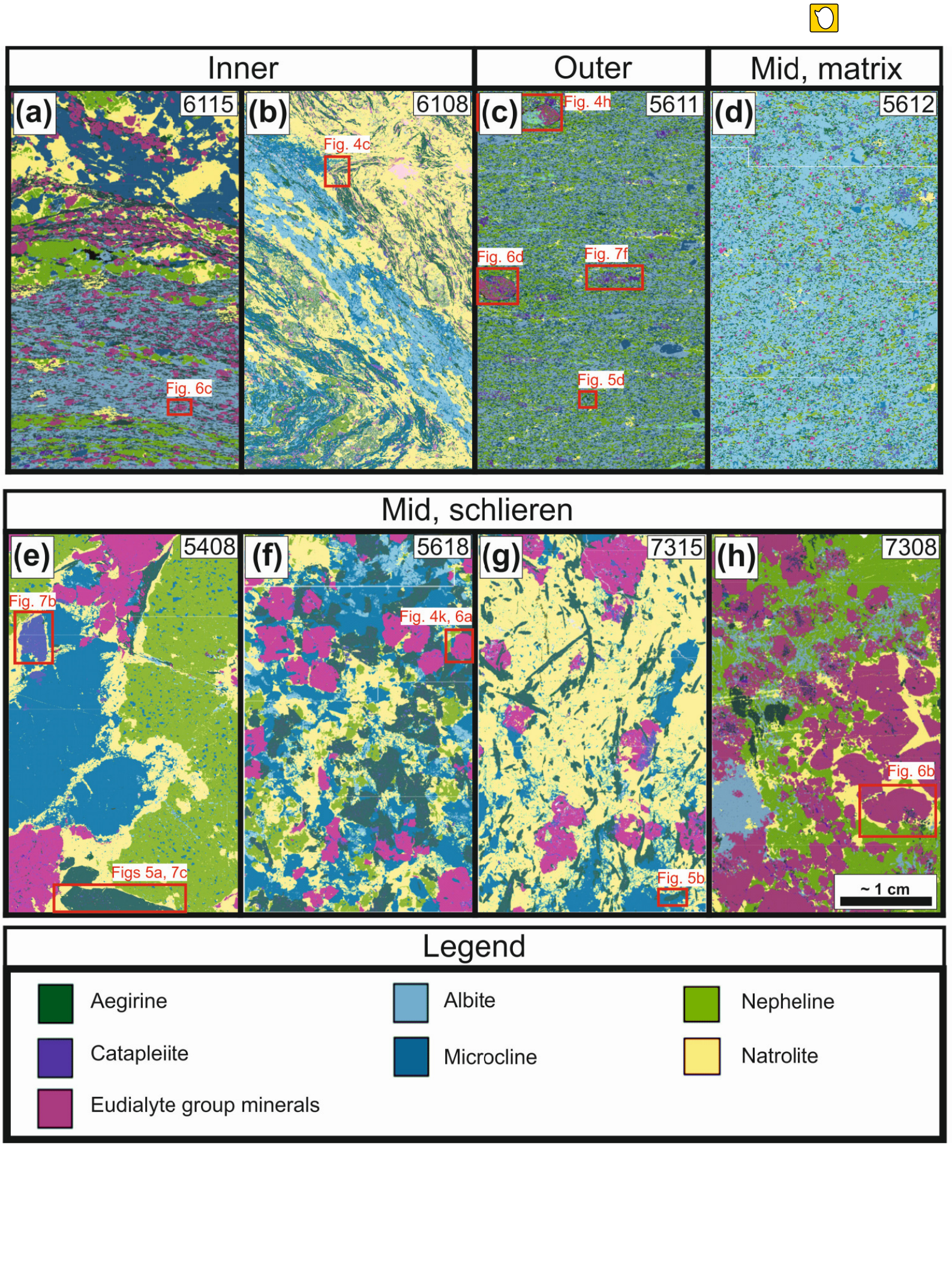
Inner
Outer
Mid, matrix
(a)
6115
Fig. 6c
(b)
6108
Fig. 4c
(c)
Fig. 4h
5611
Fig. 6d
Fig. 7f
Fig. 5d
(d)
5612
Mid, schlieren
(e)
5408
Fig. 7b
Figs 5a, 7c
(f)
5618
Fig. 4k, 6a
(g)
7315
Fig. 5b
(h)
7308
Fig. 6b
~ 1 cm
Legend
Aegirine
Albite
Nepheline
Catapleiite
Microcline
Natrolite
Eudialyte group minerals

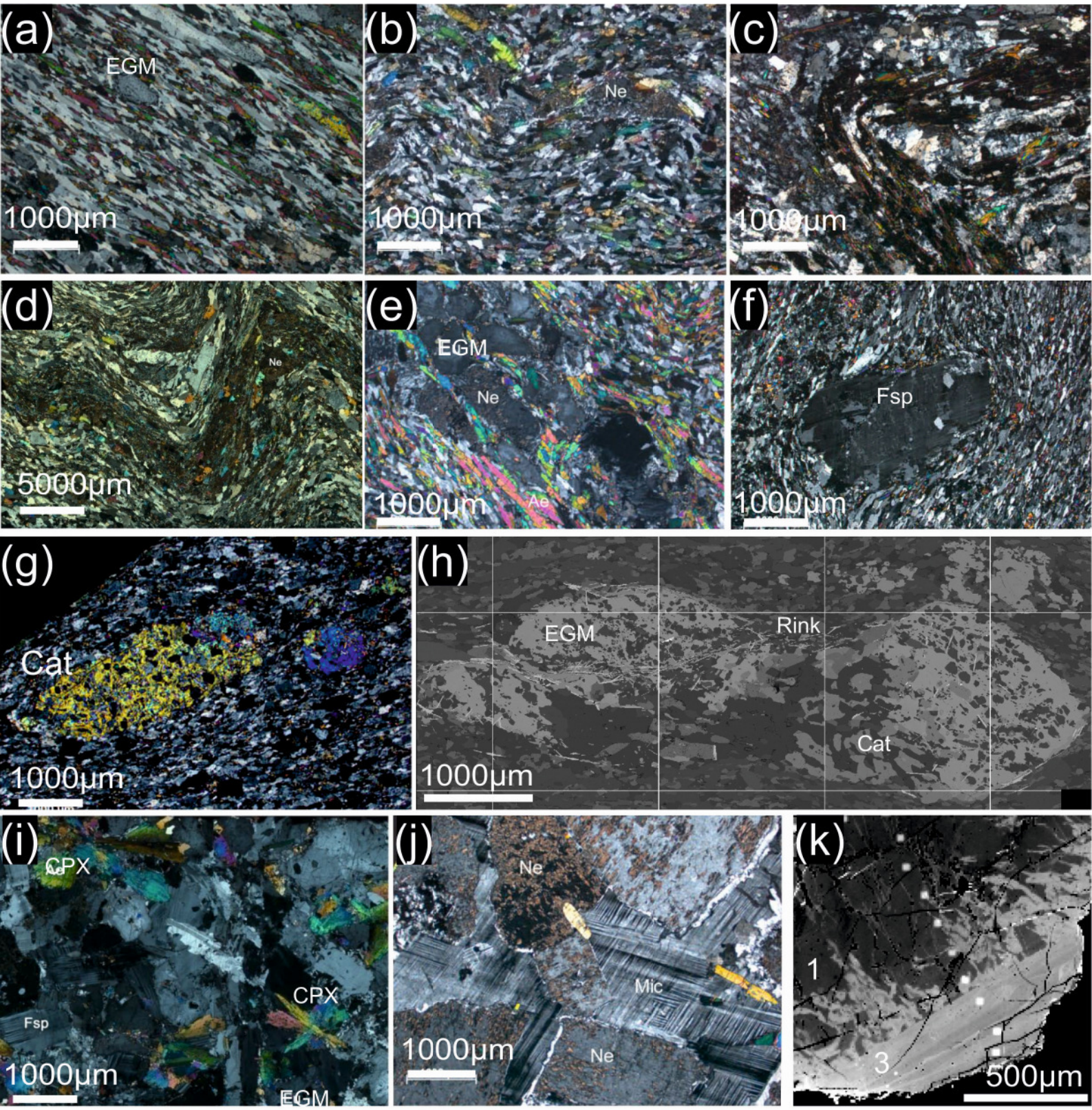
(a)
EGM
1000μm
(b)
Ne
1000μm
(c)
1000μm
(d)
Ne
5000μm
(e)
EGM
Ne
1000μm
Ae
(f)
Fsp
1000μm
(g)
Cat
1000μm
(h)
EGM
Rink
Cat
1000μm
(i)
Ae
CPX
CPX
Fsp
1000μm
EGM
(j)
Ne
Mic
1000μm
Ne
(k)
1
3
500μm

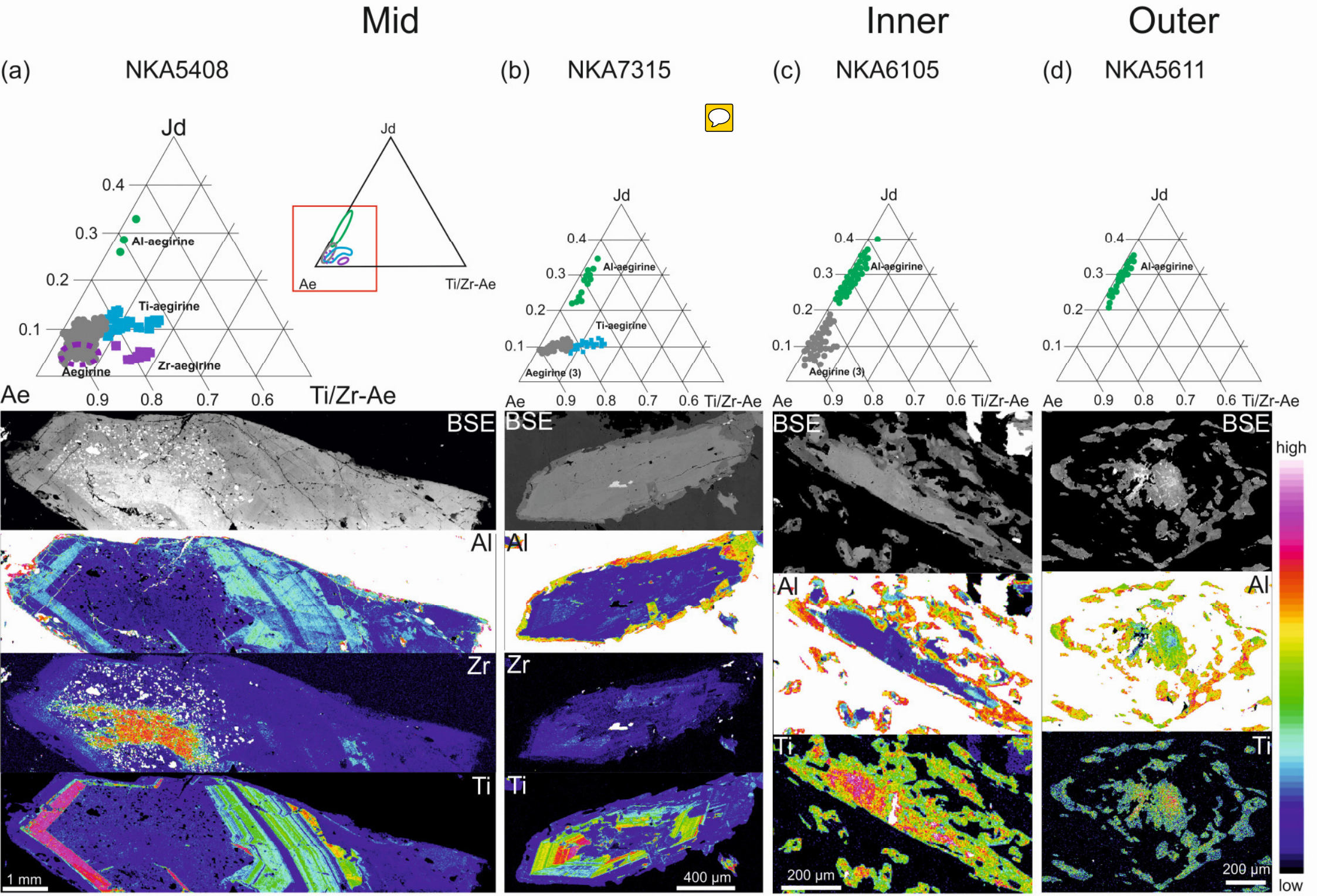
Mid
Inner
Outer
(a) NKA5408
(b) NKA7315
(c) NKA6105
(d) NKA5611
Jd
Ae
Ti/Zr-Ae
Al-aegirine
Ti-aegirine
Zr-aegirine
Aegirine
Aegirine (3)
0.4
0.3
0.2
0.1
0.9
0.8
0.7
0.6
BSE
Al
Zr
Ti
high
low
1 mm
400 μm
200 μm
200 μm

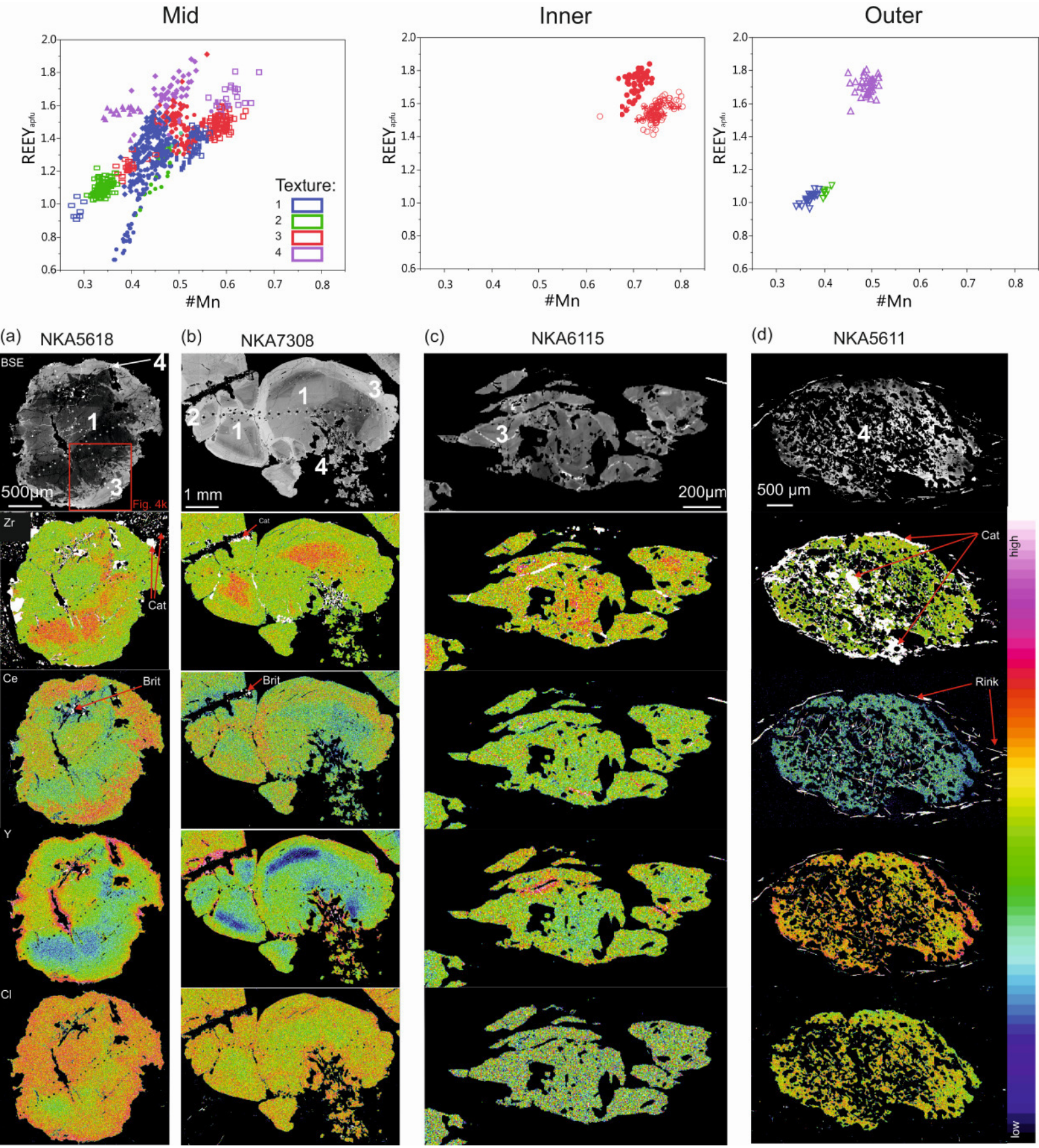
Mid
Inner
Outer
REEY apfu
#Mn
Texture:
1
2
3
4
(a) NKA5618
(b) NKA7308
(c) NKA6115
(d) NKA5611
BSE
500µm
Fig. 4k
1 mm
200µm
500 µm
Zr
Cat
Ce
Brit
Y
Cl
Rink
high
low

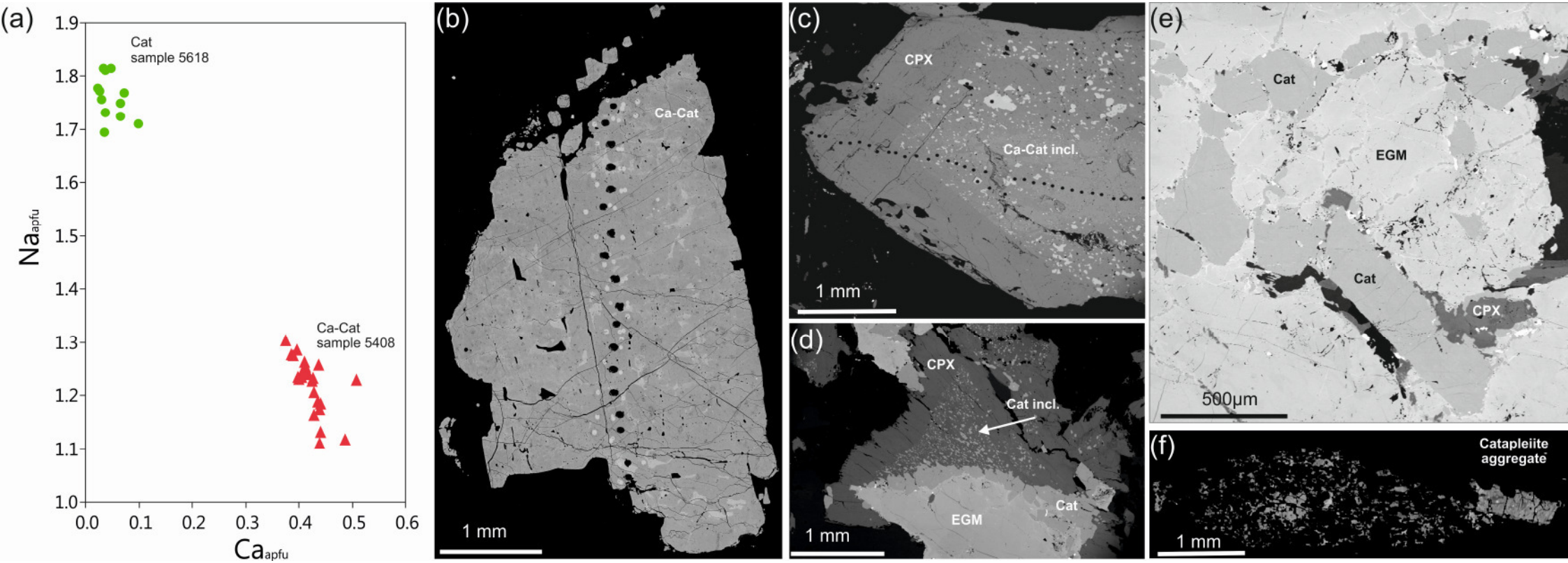
(a)
Cat
sample 5618
Ca-Cat
sample 5408
Na apfu
Ca apfu
1.9
1.8
1.7
1.6
1.5
1.4
1.3
1.2
1.1
1.0
0.0
0.1
0.2
0.3
0.4
0.5
0.6
(b)
Ca-Cat
1 mm
(c)
CPX
Ca-Cat incl.
1 mm
(d)
CPX
Cat incl.
EGM
Cat
1 mm
(e)
Cat
EGM
Cat
CPX
500µm
(f)
Catapleiite
aggregate
1 mm

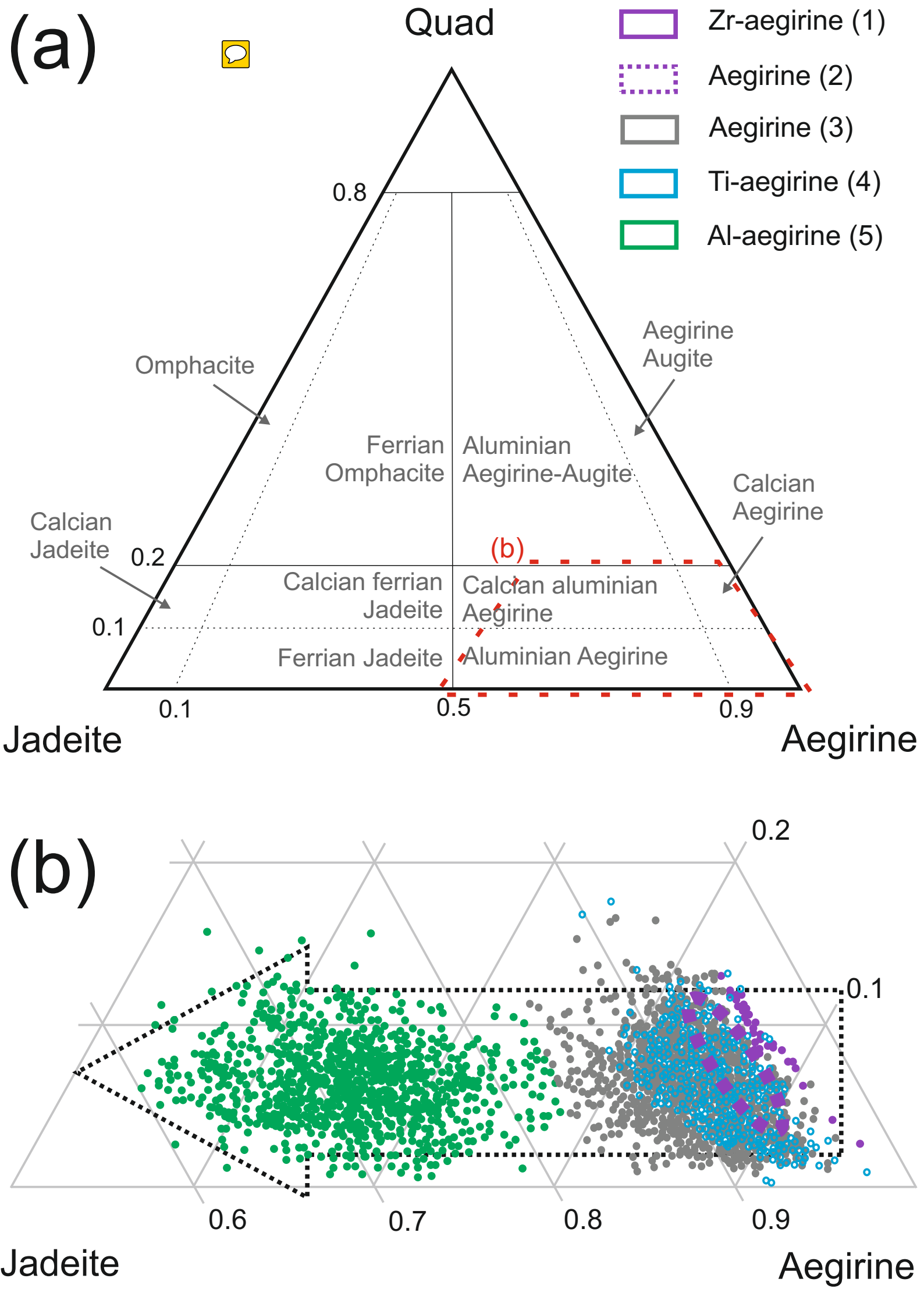
(a)
Quad
Zr-aegirine (1)
Aegirine (2)
Aegirine (3)
Ti-aegirine (4)
Al-aegirine (5)
0.8
Omphacite
Aegirine
Augite
Ferrian
Omphacite
Aluminian
Aegirine-Augite
Calcian
Aegirine
Calcian
Jadeite
0.2
(b)
Calcian ferrian
Jadeite
Calcian aluminian
Aegirine
0.1
Ferrian Jadeite
Aluminian Aegirine
0.1
0.5
0.9
Jadeite
Aegirine
(b)
0.2
0.1
0.6
0.7
0.8
0.9
Jadeite
Aegirine

(a)

(b)

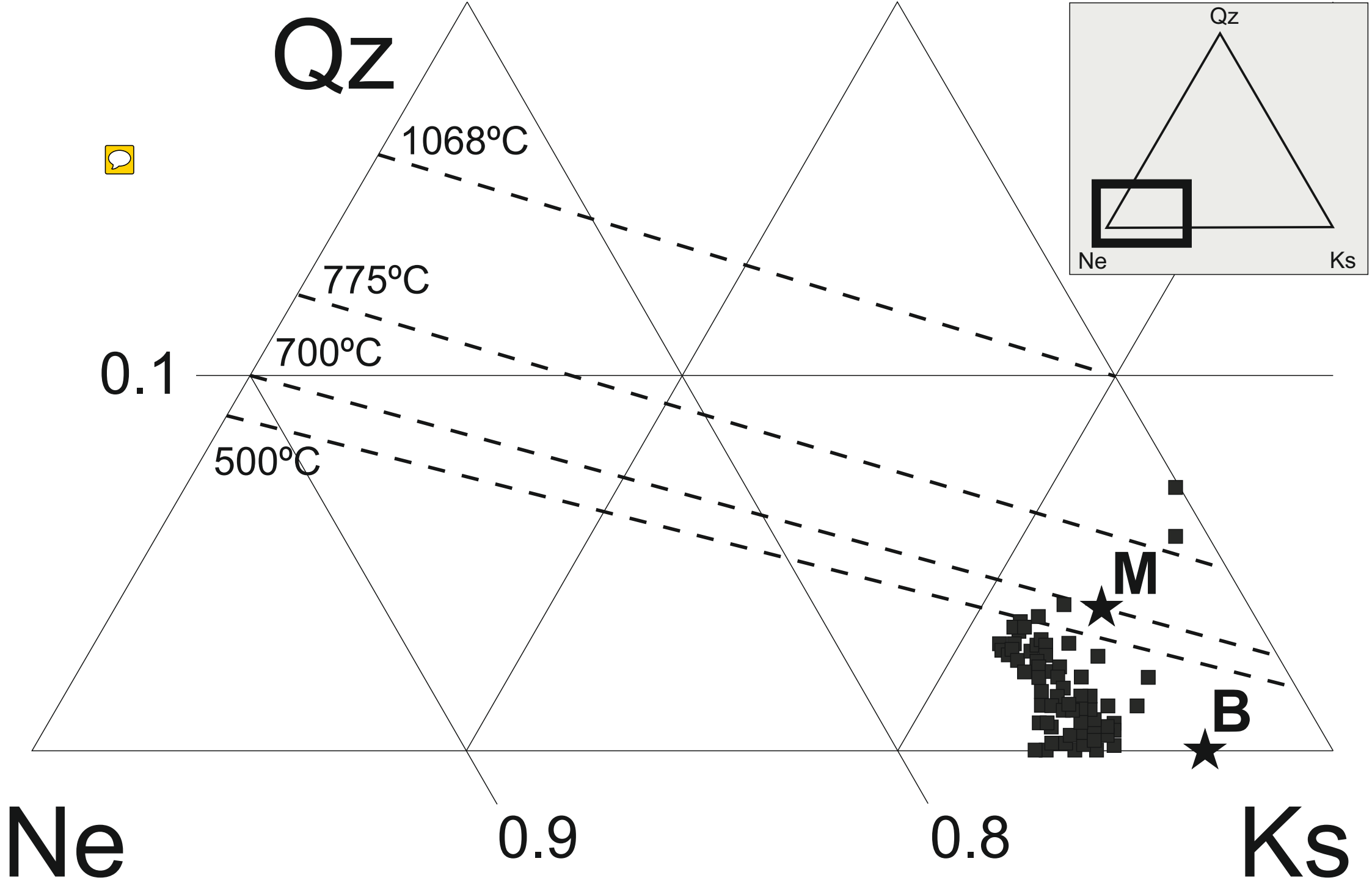
Qz
1068ºC
775ºC
700ºC
500ºC
0.1
M
B
Ne
0.9
0.8
Ks
Qz
Ne
Ks

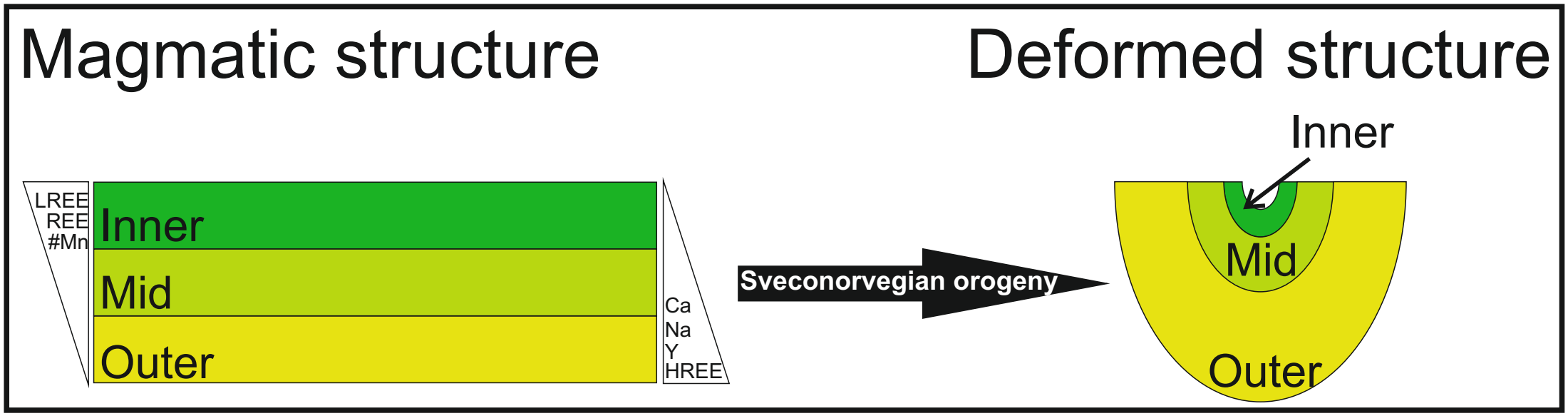
Magmatic structure
Deformed structure
LREE
REE
#Mn
Inner
Mid
Outer
Ca
Na
Y
HREE
Sveconorvegian orogeny
Inner
Mid
Outer

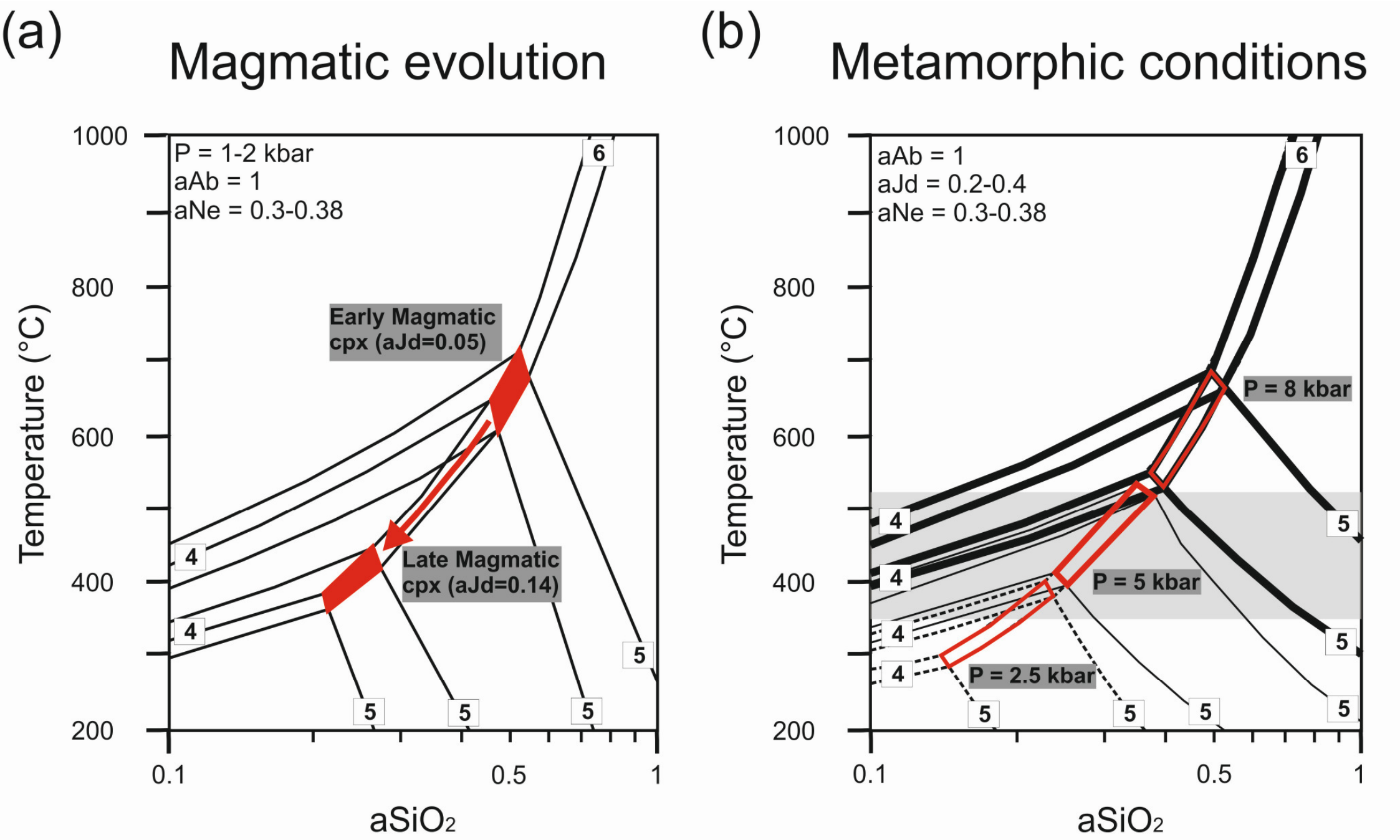
(a)
Magmatic evolution
P = 1-2 kbar
aAb = 1
aNe = 0.3-0.38
Early Magmatic
cpx (aJd=0.05)
Late Magmatic
cpx (aJd=0.14)
Temperature (°C)
aSiO2
1000
800
600
400
200
0.1
0.5
1
4
5
6
(b)
Metamorphic conditions
aAb = 1
aJd = 0.2-0.4
aNe = 0.3-0.38
P = 8 kbar
P = 5 kbar
P = 2.5 kbar
Temperature (°C)
aSiO2

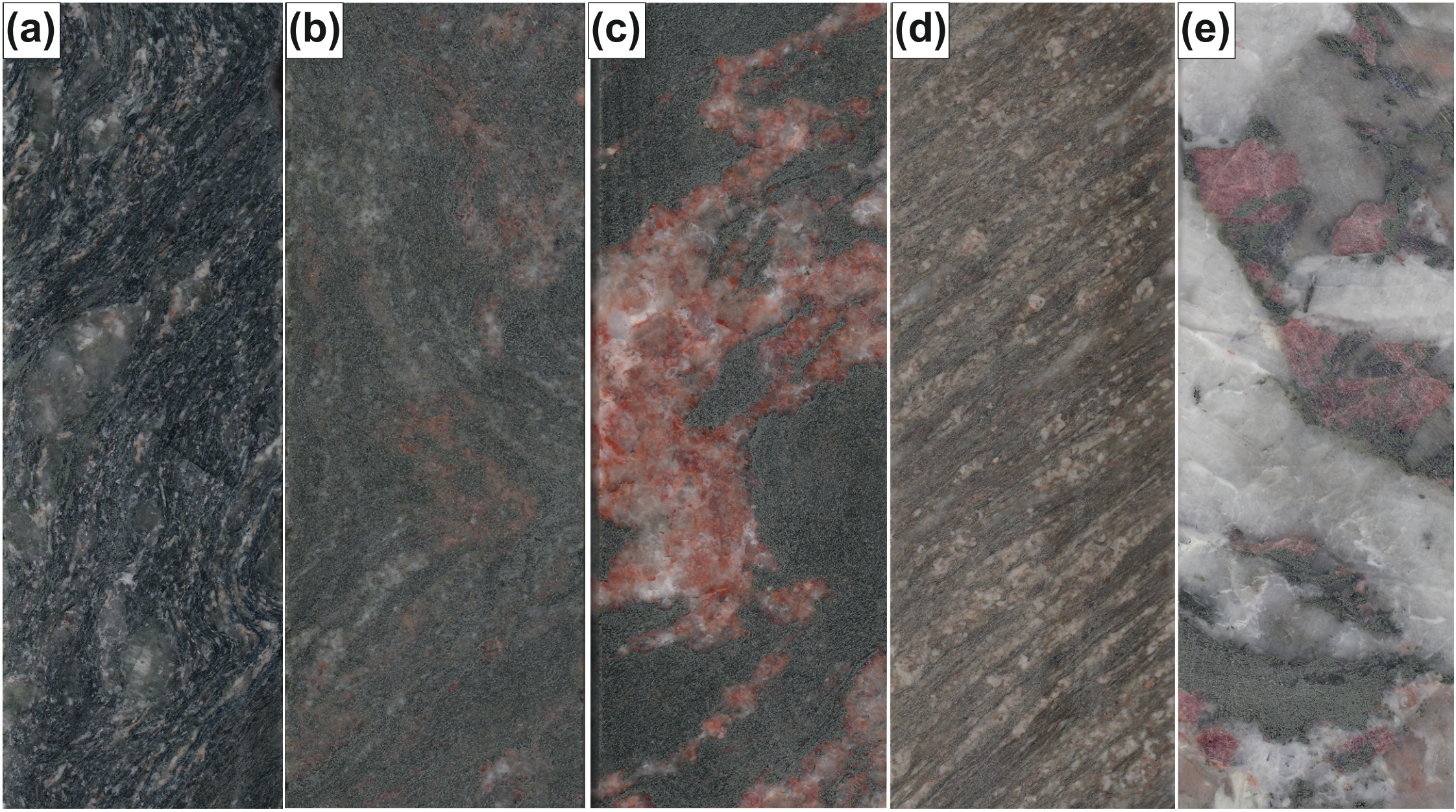
(a)
(b)
(c)
(d)
(e)

Table 1: List of investigated samples

Sample	Drill core	Position	Subunit	Analytical method (mineral)
5403	NKA 11054 P7	16.66-17.00m	Mid	MLA
5405	NKA 11054 P7	25.08-25.29m	Mid	MLA
5406	NKA 11054 P7	34.31-34.60m	Mid	MLA
5407-1	NKA 11054 P7	37.43-37.86m	Mid	MLA
5407-2	NKA 11054 P7	37.43-37.86m	Mid	MLA
5408	NKA 11054 P7	42.44-42.71m	Mid	MLA, EPMA (cpx, EGM, Cat)
5409	NKA 11054 P7	45.85-46.20m	Mid	MLA
5411	NKA 11054 P7	54.56-54.78m	Mid	MLA
5611	NKA 11056 J1	110.20-110.34m	Outer	MLA, EPMA (cpx, EGM)
5612	NKA 11056 J1	119.60-119.90m	Mid	MLA, EPMA (cpx, EGM)
5613	NKA 11056 J1	126.00-126.25m	Mid	MLA, EPMA (cpx, EGM)
5618	NKA 11056 J1	198.60-198.86m	Mid	MLA, EPMA (cpx, EGM, Cat)
5631	NKA 11056 J1	350.20-350.40m	Outer	MLA, EPMA (cpx)
6105	NKA 12061 J7	29.85-30.02m	Inner	MLA, EPMA (cpx, EGM)
6108	NKA 12061 J7	43.44-43.55m	Inner	MLA, EPMA (cpx, EGM)
6115	NKA 12061 J7	83.36-83.59m	Inner	MLA, EPMA (cpx, EGM)
6123	NKA 12061 J7	163.61-163.80m	Outer	MLA, EPMA (cpx, EGM)
6124-1	NKA 12061 J7	182.30-182.56m	Outer	MLA, EPMA (cpx)
6124-2	NKA 12061 J7	182.30-182.56m	Outer	MLA
6125	NKA 12061 J7	189.90-190.30m	Outer	MLA
7305-1	NKA 12073 P5	~ 22.94m	Mid	MLA
7305-2	NKA 12073 P5	~26.50m	Mid	MLA
7308	NKA 12073 P5	52.81-52.97m	Mid	MLA, EPMA (cpx, EGM)
7310	NKA 12073 P5	64.37-64.51m	Mid	MLA
7311	NKA 12073 P5	71.35-71.43m	Mid	MLA
7314	NKA 12073 P5	89.44-89.57m	Mid	MLA
7315	NKA 12073 P5	91.50-91.61m	Mid	MLA, EPMA (cpx, EGM)
7320	NKA 12073 P5	156.31-156.44m	Outer	MLA

MLA = Mineral Liberation Analyzer; EPMA = Electron Probe Microanalyzer; cpx = clinopyroxene; EGM = Eudialyte-group minerals; Cat = catapleiite

Table 2: Modal mineralogy of subunits of the Norra Kärr complex

	Inner N=3				Mid (Matrix) N=1	Mid (Schlieren) N=17				Outer N=7			
	Mean	CI	95% Interval			Mean	CI	95% Interval		Mean	CI	95% Interval	
wt.%		(+/-)	Min	Max			(+/-)	Min	Max		(+/-)	Min	Max
Albite	22.88	4.15	13.27	31.66	57.87	4.43	0.84	0.00	21.83	39.66	1.44	29.73	53.85
Microcline	16.80	3.05	15.21	19.03	4.41	25.13	1.85	2.98	58.98	13.17	0.43	8.35	15.83
Aegirine	17.60	3.19	15.24	19.69	19.42	18.20	1.23	2.86	34.03	13.47	0.55	9.42	17.49
Nepheline	9.39	1.70	4.83	12.72	10.30	8.84	1.14	0.02	32.98	20.15	1.61	3.17	29.14
Natrolite	22.11	4.01	12.12	36.86	2.57	27.12	1.47	12.12	51.24	8.16	1.72	0.39	27.19
Catapleiite	1.74	0.32	0.94	2.19	2.97	2.45	0.23	0.10	6.29	1.13	0.14	0.14	2.63
Eudialyte	7.25	1.32	1.11	14.43	2.19	13.39	1.15	2.70	35.39	3.81	0.37	0.38	6.25
Other REE minerals	1.80	0.33	0.07	4.96	0.25	0.14	0.01	0.04	0.43	0.11	0.03	0.00	0.46

CI = confidential interval

Table 3: Average compositions of the various clinopyroxene types of the Norra Kärr complex

	(1) Zr-aegirine				(2) Aegirine				(3) Aegirine				(4) Ti-aegirine				(5) Al-aegirine			
	Mean	CI	95% Interval		Mean	CI	95% Interval		Mean	CI	95% Interval		Mean	CI	95% Interval		Mean	CI	95% Interval	
wt.%	38		Min	Max	155		Min	Max	3053		Min	Max	541		Min	Max	1350		Min	Max
SiO_2	50.82	0.11	50.25	51.31	51.54	0.06	50.69	52.20	51.49	0.02	50.41	52.43	51.44	0.05	50.13	52.24	52.74	0.03	51.60	53.83
TiO_2	0.51	0.01	0.47	0.55	0.43	0.02	0.21	0.60	0.31	0.00	0.12	0.61	1.10	0.03	0.66	2.10	0.21	0.01	0.03	0.56
Al_2O_3	0.86	0.02	0.78	0.94	1.56	0.06	0.87	2.25	1.93	0.02	1.26	3.03	1.99	0.03	1.46	2.56	6.02	0.04	4.28	7.63
FeO	25.78	0.04	25.55	25.95	27.54	0.07	26.61	28.24	27.58	0.02	26.08	28.53	26.35	0.06	24.84	27.53	22.45	0.05	20.54	24.55
MnO	0.64	0.01	0.59	0.70	0.28	0.02	0.14	0.61	0.18	0.00	0.09	0.33	0.31	0.01	0.20	0.49	0.15	0.00	0.07	0.26
MgO	0.43	0.01	0.41	0.48	0.33	0.02	0.17	0.49	0.25	0.00	0.12	0.40	0.35	0.01	0.24	0.48	0.17	0.00	0.08	0.35
ZrO_2	3.20	0.02	3.11	3.28	0.44	0.03	0.15	0.94	0.29	0.01	0.05	0.92	0.53	0.03	0.08	1.69	0.08	0.00	0.02	0.20
CaO	1.61	0.03	1.50	1.77	1.02	0.04	0.61	1.57	0.81	0.01	0.34	1.53	0.60	0.02	0.36	1.01	0.74	0.01	0.32	1.31
Na_2O	11.84	0.05	11.54	12.13	12.32	0.04	11.73	12.95	12.43	0.01	11.86	12.90	12.52	0.02	12.11	12.86	12.76	0.01	12.20	13.26
K_2O	0.00	0.00	0.00	0.02	0.00	0.00	0.00	0.02	0.01	0.00	0.00	0.03	0.01	0.00	0.00	0.02	0.01	0.00	0.00	0.05
Total	95.69	0.14	94.98	96.39	95.45	0.08	94.48	96.35	95.27	0.02	93.78	96.44	95.19	0.06	93.52	96.56	95.33	0.04	93.87	96.50
Fe_2O_3	23.42	0.32	22.03	25.41	27.32	0.20	24.94	30.09	27.64	0.05	24.98	29.97	25.91	0.16	22.49	29.51	21.96	0.08	18.76	24.68
FeO	4.70	0.29	2.98	5.97	2.96	0.17	0.79	5.23	2.70	0.04	0.38	4.97	3.03	0.11	0.38	5.26	2.69	0.07	0.42	5.07
Ferric Total	98.04	0.14	97.31	98.94	98.19	0.08	97.22	99.19	98.04	0.02	96.59	99.22	97.79	0.06	96.37	99.00	97.53	0.04	96.04	98.73
Formulae based on 4 cations and 6 oxygens																				
Si	2.01	0.00	1.99	2.02	2.01	0.00	1.99	2.03	2.01	0.00	1.98	2.03	2.01	0.00	1.98	2.03	2.01	0.00	1.99	2.04
Al	0.04	0.00	0.04	0.04	0.07	0.00	0.04	0.10	0.09	0.00	0.06	0.14	0.09	0.00	0.07	0.12	0.27	0.00	0.19	0.34
Ti	0.02	0.00	0.01	0.02	0.01	0.00	0.01	0.02	0.01	0.00	0.00	0.02	0.03	0.00	0.02	0.06	0.01	0.00	0.00	0.02
Fe3+	0.70	0.01	0.66	0.75	0.80	0.01	0.73	0.88	0.81	0.00	0.73	0.88	0.76	0.00	0.66	0.87	0.63	0.00	0.54	0.71
Mg	0.03	0.00	0.02	0.03	0.02	0.00	0.01	0.03	0.01	0.00	0.01	0.02	0.02	0.00	0.01	0.03	0.01	0.00	0.00	0.02
Fe2+	0.16	0.01	0.10	0.20	0.10	0.01	0.03	0.17	0.09	0.00	0.01	0.16	0.10	0.00	0.01	0.17	0.09	0.00	0.01	0.16
Mn	0.02	0.00	0.02	0.02	0.01	0.00	0.00	0.02	0.01	0.00	0.00	0.01	0.01	0.00	0.01	0.02	0.00	0.00	0.00	0.01
Zr	0.06	0.00	0.06	0.06	0.01	0.00	0.00	0.02	0.01	0.00	0.00	0.02	0.01	0.00	0.00	0.03	0.00	0.00	0.00	0.00
Ca	0.07	0.00	0.06	0.08	0.04	0.00	0.03	0.07	0.03	0.00	0.01	0.06	0.02	0.00	0.01	0.04	0.03	0.00	0.01	0.05
Na	0.91	0.00	0.89	0.92	0.93	0.00	0.89	0.97	0.94	0.00	0.90	0.97	0.95	0.00	0.92	0.97	0.94	0.00	0.91	0.98
K	0.00	0.00	0.00	0.00	0.00	0.00	0.00	0.00	0.00	0.00	0.00	0.00	0.00	0.00	0.00	0.00	0.00	0.00	0.00	0.00
χ Ae	78.43	0.38	76.98	81.31	87.86	0.27	84.67	92.03	87.77	0.08	82.58	92.23	81.70	0.38	72.70	90.23	68.92	0.20	61.53	76.54
χ Jd	4.39	0.16	3.23	4.93	7.70	0.28	4.43	10.92	9.32	0.08	5.79	14.84	9.51	0.15	5.83	12.74	29.53	0.21	21.23	37.41

χ Ti-Zr-Ae	17.18	0.25	15.47	18.11	4.44	0.21	1.87	7.32	2.91	0.05	0.71	6.37	8.79	0.30	3.00	16.35	1.55	0.05	0.19	3.86

CI = confidential interval

Table 4: Average compositions of the various types of eudialyte-group minerals observed in the Norra Kärr rocks

	(1) Sector zoning				(2) Oscillatory zoning				(3) Irregular replacement textures				(4) Rims			
	Mean	CI	95% Interval		Mean	CI	95% Interval		Mean	CI	95% Interval		Mean	CI	95% Interval	
	321	(+/-)	Min	Max	180	(+/-)	Min	Max	374	(+/-)	Min	Max	139	(+/-)	Min	Max
SiO_2	51.56	0.05	50.59	52.36	51.09	0.04	50.49	51.57	51.20	0.08	49.95	52.55	50.91	0.11	49.69	51.85
TiO_2	0.16	0.00	0.08	0.22	0.09	0.00	0.06	0.14	0.16	0.00	0.07	0.21	0.12	0.01	0.04	0.20
ZrO_2	11.92	0.06	11.35	13.65	11.67	0.06	11.06	12.40	11.53	0.02	11.12	11.99	11.38	0.05	11.03	11.83
HfO_2	0.24	0.00	0.18	0.35	0.31	0.00	0.24	0.35	0.27	0.00	0.21	0.35	0.29	0.01	0.21	0.37
Al_2O_3	0.25	0.01	0.16	0.41	0.28	0.01	0.19	0.39	0.20	0.00	0.13	0.28	0.32	0.03	0.13	0.59
Nb_2O_5	0.50	0.02	0.21	0.85	0.74	0.02	0.47	1.07	0.94	0.03	0.44	1.54	0.89	0.05	0.30	1.36
La_2O_3	0.48	0.01	0.26	0.68	0.41	0.01	0.30	0.61	0.89	0.03	0.50	1.63	0.44	0.03	0.18	0.73
Ce_2O_3	1.32	0.02	0.79	1.63	0.95	0.03	0.74	1.45	2.01	0.05	1.07	2.86	0.98	0.07	0.40	1.63
Nd_2O_3+Pr_2O_3+Sm_2O_3	1.16	0.02	0.67	1.42	0.70	0.03	0.50	1.21	1.33	0.03	0.67	1.95	0.83	0.06	0.28	1.37
Tb_2O_3+Gd_2O_3+Dy_2O_3	0.69	0.01	0.32	0.88	0.68	0.01	0.56	0.79	0.67	0.01	0.48	0.89	1.03	0.03	0.76	1.29
Er_2O_3+Yb_2O_3	0.51	0.01	0.24	0.67	0.66	0.01	0.41	0.78	0.53	0.01	0.36	0.82	1.14	0.09	0.54	2.10
Y_2O_3	2.41	0.06	1.02	3.06	2.34	0.03	1.90	2.67	2.45	0.04	1.90	3.12	3.96	0.09	3.19	4.89
FeO	2.84	0.04	2.12	3.83	3.35	0.04	2.68	3.76	2.01	0.06	1.27	3.26	2.21	0.06	1.60	2.87
MnO	2.23	0.03	1.57	2.63	1.83	0.03	1.61	2.43	3.37	0.09	2.07	4.69	2.13	0.06	1.52	2.76
CaO	7.04	0.08	5.71	8.38	7.91	0.06	7.16	8.47	6.47	0.10	4.57	8.36	6.86	0.05	6.32	7.39
Na_2O	13.42	0.06	12.33	14.48	13.73	0.05	13.11	14.35	12.61	0.13	7.73	13.74	13.58	0.16	11.31	14.92
K_2O	0.46	0.01	0.19	0.63	0.35	0.01	0.21	0.51	0.50	0.01	0.26	0.95	0.46	0.02	0.28	0.73
Cl	0.36	0.01	0.29	0.59	0.68	0.03	0.31	0.93	0.35	0.01	0.28	0.88	0.41	0.02	0.23	0.56
O=Cl	0.08	0.00	0.07	0.13	0.15	0.01	0.07	0.21	0.08	0.00	0.06	0.20	0.09	0.00	0.05	0.13
Total, corrected	97.45	0.07	96.24	98.36	97.62	0.07	96.67	98.57	97.40	0.07	95.61	98.64	97.85	0.12	96.24	98.89
TREO total	4.16	0.06	2.79	4.89	3.40	0.05	2.98	4.45	5.43	0.09	3.76	6.97	4.41	0.08	3.52	5.22
Formula based on Σ(Si Al Zr Ti Hf Nb) normalized to 29 apfu																
Si	25.75	0.02	25.36	25.91	25.72	0.01	25.57	25.86	25.75	0.01	25.63	25.85	25.72	0.01	25.60	25.84
Ti	0.06	0.00	0.03	0.08	0.03	0.00	0.02	0.05	0.06	0.00	0.03	0.08	0.04	0.00	0.02	0.08
Zr	2.90	0.01	2.79	3.27	2.87	0.01	2.73	3.03	2.83	0.01	2.74	2.96	2.80	0.01	2.74	2.90
Hf	0.03	0.00	0.03	0.05	0.04	0.00	0.03	0.05	0.04	0.00	0.03	0.05	0.04	0.00	0.03	0.05
Al	0.15	0.00	0.09	0.23	0.17	0.00	0.12	0.23	0.12	0.00	0.07	0.16	0.19	0.02	0.08	0.35
Nb	0.11	0.00	0.05	0.19	0.17	0.01	0.11	0.25	0.21	0.01	0.10	0.35	0.20	0.01	0.07	0.31
La	0.09	0.00	0.05	0.12	0.08	0.00	0.06	0.11	0.17	0.01	0.09	0.30	0.08	0.01	0.03	0.14
Ce	0.24	0.00	0.14	0.30	0.18	0.00	0.14	0.27	0.37	0.01	0.20	0.54	0.18	0.01	0.07	0.30
Nd+Pr+Sm	0.21	0.00	0.12	0.26	0.13	0.00	0.09	0.22	0.24	0.01	0.12	0.36	0.15	0.01	0.05	0.25

Tb+Gd+Dy	0.06	0.00	0.03	0.07	0.06	0.00	0.05	0.07	0.06	0.00	0.04	0.07	0.09	0.00	0.06	0.11
Er+Yb	0.04	0.00	0.02	0.05	0.05	0.00	0.03	0.06	0.04	0.00	0.03	0.06	0.09	0.01	0.04	0.17
Y	0.64	0.01	0.27	0.81	0.63	0.01	0.51	0.72	0.66	0.01	0.51	0.83	1.07	0.03	0.85	1.32
Fe	1.19	0.02	0.88	1.59	1.41	0.02	1.13	1.59	0.85	0.02	0.54	1.38	0.93	0.03	0.67	1.20
Mn	0.94	0.01	0.67	1.11	0.78	0.01	0.68	1.04	1.43	0.04	0.90	2.02	0.91	0.03	0.65	1.17
Ca	3.77	0.04	2.98	4.49	4.27	0.03	3.84	4.60	3.48	0.05	2.50	4.55	3.72	0.03	3.40	4.03
Na	12.99	0.05	11.90	14.00	13.40	0.04	12.84	13.92	12.30	0.14	7.37	13.57	13.31	0.18	11.04	14.62
K	0.29	0.01	0.12	0.40	0.22	0.01	0.14	0.33	0.32	0.01	0.17	0.59	0.30	0.01	0.18	0.47
Cl	0.31	0.01	0.24	0.50	0.58	0.03	0.27	0.80	0.30	0.01	0.24	0.76	0.35	0.01	0.20	0.49

CI = confidential interval

Table 5: Catapeliite compositions from the Norra Kärr complex

	Ca-Catapleiite sample 5408, n=24				Catapleiite sample 5618, n=12			
	Mean	CI	95% Interval		Mean	CI	95% Interval	
wt %		(+/-)	Min	Max		(+/-)	Min	Max
SiO_2	45.85	0.18	45.04	46.53	46.54	0.16	46.18	46.93
TiO_2	0.02	0.00	0.01	0.03	0.03	0.01	0.02	0.05
ZrO_2	29.07	0.09	28.61	29.39	29.92	0.37	27.80	29.56
HfO_2	0.59	0.07	0.47	0.91	0.69	0.06	0.54	0.83
$REEY_2O_3$	0.41	0.03	0.30	0.56	0.46	0.05	0.31	0.58
FeO	0.20	0.13	0.04	0.95	1.10	0.55	0.10	2.80
CaO	5.99	0.18	5.41	6.99	0.68	0.20	0.35	1.30
Na_2O	9.55	0.16	8.75	10.14	13.83	0.23	13.30	14.33
K_2O	0.04	0.01	0.01	0.09	0.05	0.02	0.02	0.10
Total	91.71	0.31	90.63	93.14	92.30	0.38	91.66	93.27
H_2O (calc)	7.44	0.02	7.37	7.49	7.76	0.02	7.70	7.78
Total (incl H_2O)	99.15	0.31	98.10	100.56	100.06	0.39	99.37	101.08
Formulae based on 10 cations and 11 oxygens								
Si	3.02	0.00	3.00	3.04	3.06	0.01	3.05	3.07
Ti	0.00	0.00	0.00	0.00	0.00	0.00	0.00	0.00
Zr	0.93	0.00	0.92	0.94	0.93	0.01	0.89	0.95
Hf	0.01	0.00	0.01	0.02	0.01	0.00	0.01	0.02
REEY	0.01	0.00	0.01	0.01	0.01	0.00	0.01	0.01
Fe	0.01	0.01	0.00	0.05	0.06	0.03	0.01	0.15
Ca	0.42	0.01	0.38	0.50	0.05	0.01	0.02	0.09
Na	1.22	0.02	1.11	1.29	1.76	0.03	1.70	1.82
K	0.00	0.00	0.00	0.01	0.00	0.00	0.00	0.01
H (calc)	3.76	0.01	3.72	3.78	3.92	0.01	3.89	3.95

CI = confidential interval

Table 6: Average feldspar compositions in metasyenites from the Norra Kärr complex

	Microcline n=338				Albite n=122			
	Mean	CI	95% Interval		Mean	CI	95% Interval	
wt %		(+/-)	Min	Max		(+/-)	Min	Max
SiO_2	65.03	0.03	64.39	65.44	69.44	0.04	68.92	69.87
Al_2O_3	18.99	0.01	18.76	19.18	19.54	0.02	19.32	19.72
FeO	0.10	0.01	0.01	0.34	0.09	0.01	0.00	0.23
BaO	0.06	0.00	0.00	0.12	0.03	0.00	0.00	0.07
CaO	0.00	0.00	0.00	0.01	0.00	0.00	0.00	0.01
Na_2O	0.38	0.02	0.06	0.60	11.85	0.03	11.56	12.11
K_2O	17.15	0.03	16.81	17.64	0.10	0.01	0.05	0.17
TOTAL	101.70	0.04	100.81	102.26	101.06	0.06	100.36	101.70
Formulae based on 32 oxygens								
Si	12.03	0.01	11.92	12.11	12.74	0.01	12.64	12.82
Al	4.14	0.00	4.09	4.18	4.22	0.00	4.18	4.26
Fe^{2+}	0.02	0.00	0.00	0.05	0.01	0.00	0.00	0.03
Ca	0.00	0.00	0.00	0.00	0.00	0.00	0.00	0.00
Na	0.14	0.01	0.02	0.21	4.22	0.01	4.11	4.31
K	4.05	0.01	3.97	4.16	0.02	0.00	0.01	0.04
Ba	0.00	0.00	0.00	0.01	0.00	0.00	0.00	0.01
X_{An}	0.01	0.00	0.00	0.05	0.02	0.00	0.00	0.06
X_{Ab}	3.23	0.15	0.52	5.12	99.42	0.05	99.08	99.69
X_{Or}	96.76	0.15	94.88	99.45	0.56	0.05	0.28	0.91

CI = confidential interval

Table 7: Average nepheline, natrolite and analcime compositions from Norra Kärr rocks

	Nepheline N=108				Natrolite N=104				Analcime N=4			
	Mean	CI	95% Interval		Mean	CI	95% Interval		Mean	CI	95% Interval	
wt %		(+/-)	Min	Max		(+/-)	Min	Max		(+/-)	Min	Max
SiO_2	42.23	0.16	41.45	43.25	47.66	0.06	47.18	48.99	50.17	7.24	46.77	52.30
Al_2O_3	34.27	0.13	33.41	34.92	27.39	0.09	26.69	28.11	26.30	4.60	25.12	28.35
Fe_2O_3	0.12	0.02	0.04	0.33	0.13	0.04	0.00	0.44	0.13	0.23	0.04	0.23
BaO	0.04	0.00	0.00	0.09	0.03	0.00	0.00	0.07	0.04	0.07	0.01	0.06
CaO	0.02	0.02	0.00	0.27	0.01	0.01	0.00	0.06	0.03	0.03	0.02	0.03
Na_2O	16.08	0.10	14.92	16.52	15.24	0.04	14.92	15.60	13.50	2.64	12.25	14.17
K_2O	7.59	0.10	6.87	8.03	0.06	0.01	0.01	0.15	0.53	1.49	0.05	1.10
Total	100.35	0.09	99.66	101.07	90.53	0.12	89.52	91.66	90.71	5.05	88.51	92.52
	Formulae based on 16 oxygens				Formulae based on 10 oxygens				Formulae based on 6 oxygens			
Si	0.70	0.00	0.69	0.72	3.01	0.00	2.98	3.03	1.90	0.27	1.77	1.98
Al	0.67	0.00	0.66	0.69	2.04	0.01	1.99	2.09	1.17	0.21	1.12	1.27
Fe^{3+}	0.00	0.00	0.00	0.00	0.01	0.00	0.00	0.02	0.00	0.01	0.00	0.01
Ca	0.00	0.00	0.00	0.00	0.00	0.00	0.00	0.00	0.00	0.00	0.00	0.00
Na	0.52	0.00	0.48	0.53	1.87	0.01	1.83	1.91	0.99	0.19	0.90	1.04
K	0.16	0.00	0.15	0.17	0.00	0.00	0.00	0.01	0.03	0.07	0.00	0.05
B	-	-	-	-	0.00	0.00	0.00	0.00	0.00	0.00	0.00	0.00

CI = confidential interval

Table 8: Reintegrated compositions of Zr-aegirine (based on the composition, frequency and molar volumes of catapleite and aegirine s.str.) compared with measured compositions of Zr-aegirine core from sample 5408

	Reintergrated		Measured
Vol %	1	2	
Cpx	89	84	
Catapleiite	11	16	
SiO_2	51.07	50.94	50.83
TiO_2	0.51	0.49	0.50
Al_2O_3	1.13	1.10	0.85
FeO	25.93	25.15	25.78
MnO	0.34	0.33	0.64
ZrO_2	2.11	2.96	3.21
CaO	1.20	1.17	1.63
Na_2O	12.25	12.30	11.83
K_2O	0.01	0.01	0.00
Total	94.55	94.46	95.27